

# CRHyME (Climatic Rainfall Hydrogeological Modelling Experiment): a new model for geo-hydrological hazard assessment at the basin scale

Andrea Abbate<sup>1</sup>, Leonardo Mancusi<sup>1</sup>, Francesco Apadula<sup>1</sup>, Antonella Frigerio<sup>1</sup>, Monica Papini<sup>2</sup>, Laura Longoni<sup>2</sup>

<sup>1</sup>RSE, Ricerca Sistema Energetico, Via Rubattino 54, Milano

5 <sup>2</sup>Politecnico di Milano, Piazza Leonardo da Vinci 32, Milano

*Correspondence to:* Andrea Abbate (andrea.abbate@rse-web.it)

**Abstract.** This work presents the new model CRHyME (Climatic Rainfall Hydrogeological Modelling Experiment), a tool for geo-hydrological hazard evaluation. CRHyME is a physically based and spatially distributed model written in Python language that represents an extension of the classic hydrological models working at the basin scale. CRHyME's main focus is the simulation of rainfall-induced geo-hydrological instabilities such as shallow landslides as well as debris flows, catchment erosion, and sediment transport into the river. These phenomena are conventionally decoupled with respect to a continuous hydrological simulation while in CRHyME they are simultaneously and quantitatively evaluated within the same code through a multi-hazard approach.

CRHyME has been tested on some case studies in Italian basins. The Caldene catchment, a well-monitored basin of 27 km<sup>2</sup> located near Lecco city (Lombardy), was considered for the calibration of solid transport routine testing also the spatial scale dependence with respect to digital terrain resolution. CRHyME was applied across larger basins of the Valtellina (Alps) and Emilia's (Apennines) areas (~2600 km<sup>2</sup>) which have experienced in the recent past severe episodes of geo-hydrological instabilities triggered by heavy precipitation. CRHyME's validation has been assessed through some hydrological indexes NSE (Nash–Sutcliffe Efficiency) and RMSE (Root Mean Square Error) while for landslide phenomena the ROC (Receiver Operating Characteristic) methodology was applied. CRHyME has been able to: 1) reconstruct the surface runoff at the reference hydrometric stations located at the outlets of the basins, 2) estimate the solid transport at some hydropower reservoirs compared to the reference data, and 3) evaluate the triggering conditions of shallow landslides and debris flows. The good performance of CRHyME in terms of realistic reproduction of these catchment-scale effects was reached assuring the stability of the code, a rather fast computation, and maintaining the numerical conservativity of water and sediment balances. CRHyME is therefore a suitable tool for geo-hydrological process quantification, useful for Civil Protection multi-hazard assessment.

## 1 Introduction

Landslides, floods, and debris flows represent serious geo-hydrological hazards in mountain environments (Gariano and Guzzetti, 2016). Among them, shallow landslide, debris flow failures and soil erosion are controlled by rainfall-triggering events of varying intensity and duration (Abbate et al., 2021a) while sediment transport is a hydrologically driven process occurring at the catchment scale (Brambilla et al., 2020; Papini et al., 2017; Longoni et al., 2016; Ballio et al., 2010). Natural disasters are a critical issue in terms of economic losses and casualties (ISPRA, 2018). Only in 2020, the worldwide losses related to geohazard were quantified as 210 billion dollars and 8'200 victims (Munich Re, 2021). Among the natural disasters, the events linked to geo-hydrological phenomena, such as floods and landslides, certainly play a significant role. In Italy, a total area of 50'117 km<sup>2</sup>, which corresponds to 16.6% of the national territory is affected by high or very high landslide hazards and/or by a medium hydraulic hazard (ISPRA, 2018). In 2021, the number of victims of landslide and flood events was five and the evacuated people were around 1'000 (CNR and IRPI, 2021). Northern Italy has the highest mortality rate caused by landslides and floods in the country, varying in the range of 0.034 for Emilia Romagna and 0.085 for Piedmont (number of deaths and missing people per 100'000 people in one year).

Geo-hydrological hazards are complex and heterogeneous phenomena, so a great effort has been made in the past to understand their dynamics and triggering factors (Gariano and Guzzetti, 2016; Ceriani et al., 1994; Gao et al., 2018; Kim et al., 2020). There are many studies concerning shallow landslide dynamics in the literature, based both on laboratory and field experiments (Guzzetti et al., 2007; Herrera, 2019; Meisina et al., 2013; Crosta et al., 2003; Iverson, 2000; Ivanov et al., 2020b), which highlight rainfall as the main triggering factor for this type of phenomenon. However, in the literature is still missing a widely accepted methodology that can strongly connect the different components that interplay in geo-hydrological hazard generation and evolution (Gariano and Guzzetti, 2016; Bordoni et al., 2015). In this context, shallow landslides, debris flow and solid transport are primarily driven by superficial soil water balance that influences the runoff generation through the infiltration mechanisms (Abbate et al., 2019).

This work will illustrate the potentialities of a new physically-based geo-hydrological model called CRHyME. CRHyME is an extension of a classical rainfall-runoff hydrological model where also geo-morphological dynamic aspects are taken into account. From the analysis of the literature (De Vita et al., 2018; Bemporad et al., 1997; Roo et al., 1996; Schellekens et al., 2020; Angeli et al., 1998; Gleick, 1989; Sutanudjaja et al., 2018; Van Der Knijff et al., 2010; Devia et al., 2015; Moges et al., 2021), rarely the two aspects have been jointly taken into account. Lots of hydrological models adopted worldwide are interested mainly in flood propagation and water balance assessment (Sutanudjaja et al., 2018). One of their main limitations is that they are rather advanced in the hydrological part, proposing a very detailed description of the hydrological cycle while geo-hydrological hazards interaction is hardly taken into account (Shobe et al., 2017; Strauch et al., 2018; Campforts et al., 2020). Up to now, there are still few examples that can include the triggering analysis of shallow landslide and debris flow, or a solid transport quantification (Roo et al., 1996; Gariano and Guzzetti, 2016; Alvioli et al., 2018). In literature, some of them consider the erosion and solid transport mechanisms at the watershed scale (Vetsch et al., 2018; Tangi et al., 2019; Roo et al., 1996; Papini et al., 2017) while the stability of natural slopes is still not properly included in distributed hydrological models and vice-versa. The slope stability or debris flow analysis is computed inside dedicated models such as those (Iverson, 2000; Scheidl and Rickenmann, 2011; Harp et al., 2006; Milledge et al., 2014; Montrasio, 2008; Takahashi, 2009) that take into account some aspect of the hydrological cycle but they are generally not fully integrated into a rainfall-runoff routine. Moreover, several models can be applied to a few cases due to other limitations such as input data requirements, the scale of simulation and the data resolution (Devia et al., 2015; Moges et al., 2021).

Fortunately, some advances in this direction have been made in very recent years. In this regard, CHASM (Combined Hydrology and Stability Model) (Bozzolan et al., 2020) and Landlab (Strauch et al., 2018) represent the two latest modelling frameworks that have addressed the need to start evaluating the geo-hydrological hazard and risks considering also hydrological and climatic aspects. The new methodological approaches shown by CHASM and Landlab models have been assessed thanks to the progressively increasing data availability for GIS (Geographical Information Systems) on a worldwide scale and thanks to the recent improvements in computer programming for environmental systems. Indeed, the creation of efficient and open-source built-in functions for different language programs, such as Matlab, C++ or Python, has sped up and facilitated the implementation of self-made land-surface models. These functions have been already successfully implemented by PCR-GLOBWB-2 (Sutanudjaja et al., 2018) and WFLOW (Schellekens et al., 2020) models, as well as in the European hydrological model LISFLOOD (Van Der Knijff et al., 2010) and OPENLISEM (Roo et al., 1996).

In this paramount of software solutions and approaches, a comprehensive multi-hazard model specifically designed for evaluating geo-hydrological threats is still needed. Geo-hydrological processes are many and generally happen simultaneously at watershed scale. They need to be modelled together to better know their mutual influences and feedback, trying to overcome the theoretical subdivisions existing in the literature's methodologies currently adopted. Starting from this point, the main motivations aimed at the construction of the new CRHyME code are here presented:

- Build an integrated but versatile model for simulating rainfall-induced geo-hydrological processes (flood, erosion, sediment transport and shallow landslide triggering);

- Allow fast and efficient calculations within a spatially distributed model designed to operate at catchment scale without constraints on spatial and temporal input data resolution;
- Implementation of a code inside a robust framework, using Opens Source Python libraries which enable fast coding and easy sub-module modifications/integrations;
- Code compatibility for assimilating input data from Opens Source datasets available at a worldwide scale, permitting a simulation reproducibly in whatever catchments;

85

90

Starting from these considerations and taking inspiration from analogue models cited before, CRHyME (Figure 1) was developed to try to fill the existing gaps and issues, improving overall geo-hydrological modelling. This paper presents the main features and several applications of the code. Structure and constitutive equations are reported in the Material and Method section. Then some case studies developed across Italian territory were taken into account for the calibration and validation of the new model. In the Result section the main outcomes of CRHyME applications are reported and they are extensively commented on within the Discussion and Conclusions sections.

## 2 Material and Methods

95

In this paragraph, the CRHyME model peculiarities are illustrated: the main features, the sub-module structure and their constitutive equations, the input dataset for its initialization, and a presentation of the test cases.

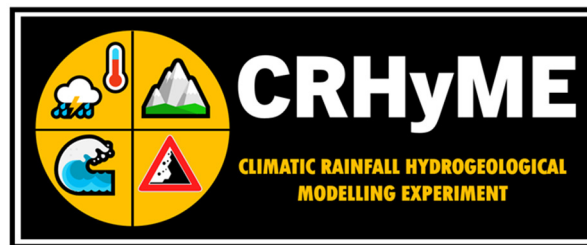


Figure 1: CRHyME logo.

### 2.1 Model main features

100

CRHyME aims to model together hydrological and geological processes at the catchment scale, e.g. floods and landslides. Historically, these processes have been studied separately but in CRHyME are evaluated simultaneously: the bed-load sediment transport has been described considering the Erosion Potential Method (EPM) for simulating erosion sources (Longoni et al., 2016; Brambilla et al., 2020; Milanesi et al., 2015; Ivanov et al., 2020a) and the stream power laws for defining the transport capacity of the rivers (Vetsch et al., 2018); the shallow landslide failure assessment was carried out considering 4 infinite-slope stability models (Iverson, 2000; Montrasio, 2008; Harp et al., 2006; Milledge et al., 2014); the debris flow stability was evaluated through the theory proposed by (Takahashi, 2009) since, according to Theule, 2012, Jakob and Jordan, 2001, they are complex phenomena which can behave intermediately among floods and landslides.

105

110

115

The CRHyME's code architecture is partially inherited by the PCR-GLOBWB-2 model (Sutanudjaja et al., 2018). This model is characterized by a well-organized framework that could guarantee the robustness and the stability of the code, fast modelling and reduced time consumption thanks to embedded function parallelization, no constraints on the spatial and temporal resolution of the input data, and easy code adaptation for new features. The PCR-GLOBWB-2 engine is based on PCRaster libraries (Karssenberget al., 2010; Pebesma et al., 2007). The PCRaster Python libraries offer a series of standard functions for hydrological processing on calculation grids which can be easily "called" via Python scripts to perform individual operations. CRHyME's framework is organized within a modular structure which enables easier single-model updating to introduce new features. Python programming language is open-source, and its flexibility permits to manage of large

meteorological and climatic databases which are essential for computing event-based and long-term simulations. All these features has been included, adapted, reworked, and improved inside CRHyME.

## 2.2 Model structure

The CRHyME model is composed of a series of modules that run successively in a loop as represented in Figure 2. The simulations are initialized from a pre-compiled “.INI” file (see Appendix A) where all the settings and input data are specified (see Appendix B). The modules are:

1. CLIMA: elaborates precipitation and temperature data from reanalysis and climate datasets, using the “NetCDF” (Network Common Data Form, “.netcdf”) format (Bonanno et al., 2019; Sutanudjaja et al., 2018);
2. METEO: elaborates precipitation and temperature data from ground-based weather stations using the PCRaster standard format “.tss” (Karssenberget al., 2010) for data series and calculates the evapotranspiration;
3. INTERCEPTION: excludes from net precipitation the canopy interception and computes the snow dynamic;
4. LANDSURFACE: evaluates the water balance in the superficial soil giving information about runoff, soil moisture and percolation losses;
5. GROUNDWATER: evaluates the water balance in the groundwater layer;
6. ROUTING: calculates the runoff routing across the watershed;
7. LANDSLIDE: identifies the triggering conditions for landslides and debris flows, and calculates erosion and bed-load sediment transport in rivers.

The first 6 modules constitute the “hydrological module” and are intended to evaluate the hydrological cycle while the “landslide module” is the CRHyME’s novelty where slope instability conditions and sediment transport dynamics are simulated considering the computed soil moisture and the runoff respectively.

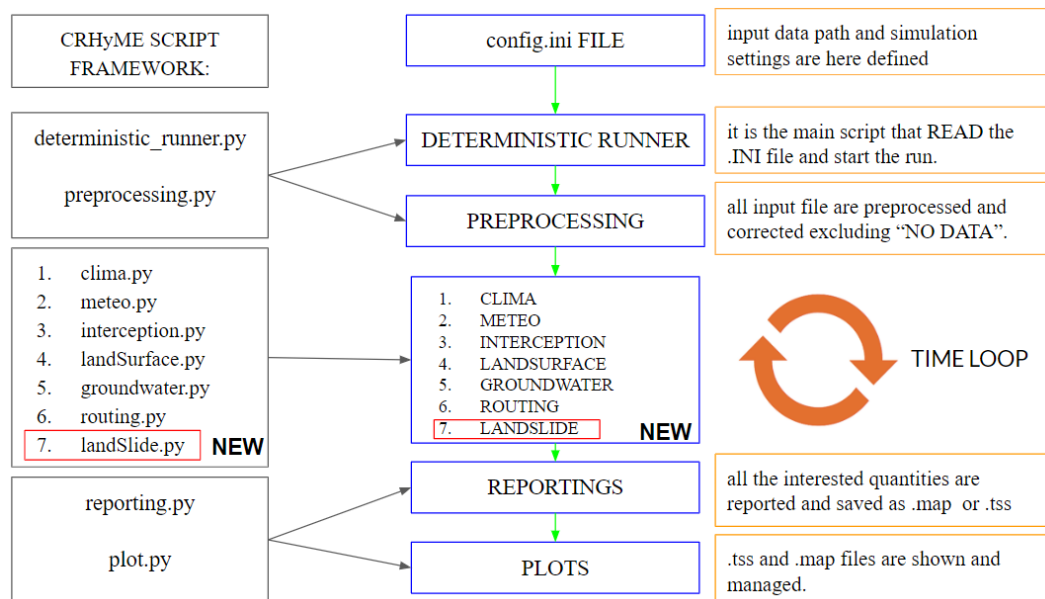


**Figure 2: Framework of the new model CRHyME. Main Python scripts are listed explaining their function and their link with the other parts of the code. For further details see Appendix A and B.**

The PCRaster libraries implemented in CRHyME have the advantage of being fully parallelized to work with multicore processors (Karssenberget al., 2010). This is an important aspect of our code that permits us to decrease sharply the time-consuming of each simulation. The intrinsic parallelization of the PCRaster libraries simplifies and facilitates code maintenance and updating, without any further parallelization optimizations. In Table 1 the operating time calculation ranked for the model CRHyME is reported for different numbers of core processors (worker thread).

CPU cores	PCRaster N° Worker Thread	Single Operation on LANDSURFACE Module with a large file (10'000 cells)	Single Cycle (1° to 7° Module) of Model Iteration with a large file (10'000 cells)
2 cores	2	4.07 s	Around 20 – 25 s
4 cores	4	1.48 s	Around 8 – 10 s
8 cores	8	1.05 s	Around 5 – 6 s

**Table 1: Performances of the CRHyME model working on different CPU core sets. It can be noticed that by increasing the number of cores available, the computation time for a particular operation can drop significantly.**

145

### 2.2.1 Model initialization

The choice of a suitable digital terrain model (DTM or DEM) is the fundamental starting point for CRHyME's code. From DTM all the essential data listed in the ".INI" file are derived: the "clone.map", a 0-1 mask that defines the computational domain; the "ldd.map", the local drain direction map that defines the flow directions (Karszenberg et al., 2010; Pebesma et al., 2007). In CRHyME, the HydroSHEDS DTM (Hydrological data and maps based on Shuttle Elevation Derivatives at multiple Scales) (Lehner et al., 2008) was selected as a reference. The HydroSHEDS DTM is designed specifically for hydrological models and has been already pre-processed to guarantee the flow connectivity of the river network (hydrologically conditioned). Its spatial resolution is about 3-sec degree, which corresponds approximately to about 90 m at the equator, and it was retained sufficiently accurately for medium-scale catchment analysis. Using the PCRaster functions, the 'flow accumulation', the 'slope', the 'curvature' and the 'slope aspect' were reconstructed immediately from HydroSHED DTM. In addition to these morphological data, other layers are required in CRHyME for geo-hydrological assessment:

150

155

- the Corine Land Cover data (<https://land.copernicus.eu>) (Girard et al., 2018) is the European inventory of landcover that was considered for defining vegetation interception and soil infiltration coefficients, spatial evapotranspiration flux and root cohesion for landslide stability;
- the Soil Grids data at 250 m resolution from the world database ISRIC (International Soil Reference and Information Centre) — World Soil Information (<https://maps.isric.org/>) (Hengl et al., 2017), were considered for assessing soil physical properties such as depth and soil composition which are implemented inside infiltration, percolation, erosion and landslide stability routines;
- the hydraulic properties of soils, such as the permeability and porosity, from the European Soil Data Centre (ESDAC) database (<https://esdac.jrc.ec.europa.eu/>) and other worldwide repositories (Tóth et al., 2017; Ross et al., 2018; Huscroft et al., 2018), were considered for assessing superficial and groundwater hydrological balance.

160

165

The datasets here described are freely available for the entire European area, but analogous can be found for other continents. Since they are provided with an open-source licence they can be implemented without restrictions. This choice aims to extend and generalise as much as possible the reproducibility of CRHyME's simulations in any worldwide catchments without any constraint on territorial input data. Moreover, the availability of free Web Feature Service (WFS) and Web Coverage Service (WCS) services allows to download them easily, speeding up CRHyME initialization.

170

Temperature and rainfall data required by simulations were gathered from ground-based meteorological stations (Rete Monitoraggio ARPA Lombardia; Rete Monitoraggio ARPA Emilia) and reanalysis databases available locally (Bonanno et al., 2019). Temperature fields were built by combining the data series at each timestep, estimating the regression coefficient with respect to the station elevation and then using the DTM information to calculate the temperature distribution (Daly et al., 1997; Chow et al., 1988). For rain gauge precipitation, a simple IDW (Inverse Weight Distance) interpolator was implemented with a distance exponent equal to 2 while for rainfall data coming reanalysis data, a simple nearest-neighbour algorithm has been adopted to downscale the precipitation field at DTM resolution (Daly et al., 1997; Chow et al., 1988; Abbate et al., 2021b; Terzago et al., 2018). CRHyME's timestep required for completing a single loop of all internal modules (Figure 2) was assumed to be equal to the meteorological forcings timestep and could vary from a minimum of 5 min up to a maximum of 1 day. In this current work, the timestep selected for CRHyME's computations is 1 day.

175

180

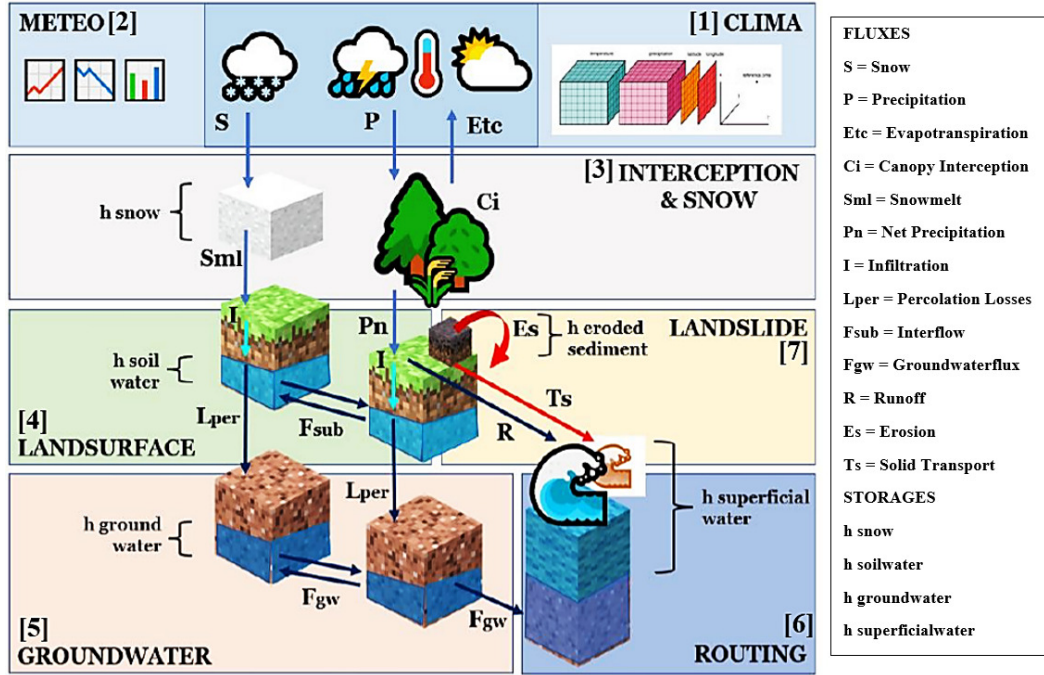


Figure 3: Scheme of the soil water and sediment balances and related mass-fluxes implemented in CRHyME. Fluxes and Storage variables constituting the model are listed.

185

### 2.2.2 Hydrological module and equations

The hydrological modules (Figures 2 and 3, from 1 to 6) evaluate the processes of transformation inflows-outflows using input maps of weather forcings consisting of precipitation [ $\text{mm timestep}^{-1}$ ] and average, maximum, and minimum temperature [ $^{\circ}\text{C}$ ]. In CRHyME each cell of the terrain domain is considered like a tank that communicates in cascade to the others following the downstream river network (Brambilla et al., 2020; Roo et al., 1996; Sutanudjaja et al., 2018). Hydrological balance is schematized considering 4 imaginary layers where water can be temporarily stored:

190

1. Snow Storage, Eq. (1) where the snow balance is assessed by  $h_{\text{snow}}(t)$  variable, [mm],
2. Superficial Soil Storage, Eq. (2) and (3) where soil infiltration is computed and the superficial soil balance is assessed by  $h_{\text{soilwater}}(t)$  variable, [mm],
3. Groundwater Soil Storage, Eq. (5) where the groundwater balance is assessed by  $h_{\text{groundwater}}(t)$  variable, [mm],
4. Runoff Storage, Eq. (6) where the runoff generated by an excess of infiltration and exfiltration is routed across the catchment and described by  $h_{\text{runoff}}(t)$ , [mm].

195

The superficial soil storage is the core of hydrological balance assessment since is the place where all the water mass fluxes, in [ $\text{mm timestep}^{-1}$ ], are exchanged between atmosphere and terrain. Balances are schematized by Eq.(1), Eq. (2) and Eq. (3).

200

- Infiltration balance in Eq. (2) establishes the net water volume  $I(t)$  that enters the soil. From precipitation  $P(t)$  is evaluated by the net precipitation  $P_n(t)$  arriving at the terrain surface subtracting the part of the rainfall intercepted by tree leaves, e.g. Canopy Interceptions  $C_i(t)$  (Li et al., 2017; Nazari et al., 2019). When the temperature is  $< 0^{\circ}\text{C}$ , all the precipitation is stored as snowpack  $h_{\text{snow}}(t)$  Eq. (1) and released aftermath as snowmelt contribute  $S_{\text{ml}}(t)$  when temperature increases above  $0^{\circ}\text{C}$  following a degree-day approach (Chow et al., 1988; Cazorzi and Dalla Fontana, 1996).  $I(t)$  is estimated directly using the common infiltration methods proposed by Horton and SCS-CN (Chow et al., 1988; Chen and Young, 2006; Mishra et al., 2003; Morbidelli et al., 2018; Ravi et al., 1998; Smith and Parlange, 1978; Ross et al., 2018) and the runoff generated by an excess of precipitation at the surface  $R(t)$ , is obtained by the difference of  $P_n(t) - I(t)$ ;

205

- 210 Superficial soil moisture balance in Eq. (3) permits to evaluate the quantity  $S_m(t)$  which is expressed dimensionless as a ratio between  $h_{soilwater}(t)$  [mm] and the product of terrain porosity  $n$  and the superficial soil depth ( $depth_{soil}$ ). Porosity and superficial soil depth are determined respectively from (Tóth et al., 2017; Ross et al., 2018; Huscroft et al., 2018) and (Hengl et al., 2017) databases. The other terms of the water balance are:
- ETc(t) evapotranspiration losses according to Hargreaves and Penman-Montheit formulations suggested by FAO guidelines (Raziei and Pereira, 2013; Allan et al., 1998);
  - 215 ○  $L_{per}(t)$  percolation losses are part of the volume that goes to the groundwater layer, evaluated as a function of the soil water balance in unsaturated conditions using Van Genuchten's functions and parameters (Jie et al., 2016; Van Genuchten, 1980; Daly et al., 2017; Groenendyk et al., 2015; Vitvar et al., 2002; Jackson et al., 2014; Klaus and Jackson, 2018);
  - Exfiltration  $Ex(t)$  is the leakage of water on the surface that occurs after the complete saturation of the superficial soil storage (ponding);
  - 220 ○  $F_{sub}(t)$ , expressed in [ $m^3 s^{-1}$ ], is the sub-surface lateral fluxes generated inside the superficial soil layer through the Dupuit approximation of the Darcy law for water filtration in soils. Here is a correction of the saturated permeability  $K_s$  [ $m s^{-1}$ ] considering the relative permeability  $K_r$  [-] caused by the partial saturation conditions has been included in the formula (Van Genuchten, 1980).  $\Delta x$  and  $\Delta y$  represent the cell dimensions in [m].
  - 225

$\frac{dh_{snow}(t)}{dt} \cong \frac{\Delta h_{snow}(t)}{\Delta t} = S(t) - S_{ml}(t)$	(1)
$I(t) = (P(t) - C_I(t) + S_{ml}(t)) - R(t) = P_n(t) - R(t)$	(2)
$\frac{d(S_m(t) * depth_{soil} * n)}{dt} = \frac{dh_{soilwater}(t)}{dt} \cong \frac{\Delta h_{soilwater}(t)}{\Delta t} \pm \frac{F_{sub}(t)}{\Delta x * \Delta y} = I(t) - ETc(t) - Ex(t) - L_{per}(t)$	(3)

230 The groundwater reservoir depth ( $depth_{GW}$ ) has been modelled considering a spatial distribution described in Eq. (4) (Fan et al., 2007; de Graaf et al., 2015; Pelletier et al., 2016). According to these studies, as the superficial slope increases, the aquifer depth is reduced until it reaches the minimum value of 0 m, e.g., corresponding to the condition of complete absence.

$depth_{GW} = a / (1 + b * slope)$	(4)
------------------------------------	-----

235 In Eq. (4) the slope is expressed as a tangent to the angle of inclination of the surface while  $a$  and  $b$  represent coefficients that are distinguished according to the depths of interest: where the depth of the bedrock is supposed to be low ( $< 10$  m, superficial bedrock), the suggested parameters are  $a = 20$  and  $b = 125$ , while if the bedrock depth is significative ( $> 10$  m, deep regolith)  $a = 120$  and  $b = 150$ . In CRHyME a rather intermediate condition has been adopted between superficial bedrock and deep regolith, therefore the parameters adopted are the following:  $a = 200$  and  $b = 125$ . This approximation has appeared sufficiently accurate concerning the fact that currently available data on groundwater aquifer depth and hydrogeology parameters are rather approximated, uncertain and with low resolution (Kobierska et al., 2015; Zomlot et al., 2015; Hayashi, 2020; Huscroft et al., 2018).

$\frac{dh_{groundwater}(t)}{dt} \cong \frac{\Delta h_{groundwater}(t)}{\Delta t} \pm \frac{F_{GW}(t)}{\Delta x * \Delta y} = L_{per}(t) - Ex_{GW}(t)$	(5)
---	-----

240

The groundwater table is generated by the percolated water  $L_{per}(t)$  coming from the upper layer Eq. (5). The groundwater lateral flow  $F_{GW}(t)$ , expressed in  $[m^3 s^{-1}]$ , is then calculated using the Dupuit approximation according to which the filtration rate is given by the product of hydraulic permeability  $K_s$  for the tangent of the slope of the impermeable substrate, supposed parallel to the slope (Klaus and Jackson, 2018; Anderson, 2005; Bresciani et al., 2014).  $Ex_{GW}(t)$  e.g., groundwater exfiltration, is the term that describes the leakage of water after the complete saturation of the groundwater storage, simulating the water springs.

$\frac{dh_{runoff}(t)}{dt} \cong \frac{\Delta h_{runoff}(t)}{\Delta t} \pm \frac{F_{kin-dyn}(t)}{\Delta x * \Delta y} = R(t) + Ex(t) + Ex_{GW}(t)$	(6)
--	-----

Superficial runoff is defined as the sum of  $R(t)$ ,  $Ex(t)$  and  $Ex_{GW}(t)$  and it is stored in  $h_{runoff}(t)$  in Eq. (6).  $h_{runoff}(t)$  is propagated across the overland surface along the lines of maximum slope and inside the river network using two possible methods available in PCRaster libraries that are deputed for the flow routing process (Chow et al., 1988; Lee and Pin Chun, 2012; Collischonn et al., 2017; Bancheri et al., 2020): kinematic and dynamic  $F_{kin-dyn}(t)$  derived from the simplification of De Saint Venant's one-dimensional equations of motion, expressed in  $[m^3 s^{-1}]$ . The first is generally applied in sections where the slopes are accentuated so it is possible to approximate the hydraulic gradient with the slope of the channel (Chow et al., 1988). The second instead introduces further terms that allow a better simulation of the outflow in correspondence to the flat areas when the other terms of the De Saint Venant equation are no longer negligible (Chow et al., 1988), but requires precise information about the geometry of rivers sections to carry out the flood wave propagation (Karszenberg et al., 2010).

### 2.2.3 Geo-hydrological module and equations

To study geo-hydrological instability it is of paramount importance to analyse the triggering causes of landslides and the dynamic of erosion and sediment transport processes (Guzzetti et al., 2005; Remondo et al., 2005; Montrasio and Valentino, 2016; Bovolo and Bathurst, 2012). For this purpose, an ad hoc new “landslide module” (Figure 3, n° 7) has been developed in CRHyME.

#### 2.2.3.1 Stability models for shallow landslides and debris flows

Shallow landslide triggering is strongly correlated with meteorological and climatic forcing (Abbate et al., 2021a). The abrupt modifications of the local hydrology with the alternation of dry and wet conditions of soil induced by precipitation are responsible for undermining the stability of the slopes (Iverson, 2000; Chen and Young, 2006). Here are described briefly the four stability models included in CRHyME: 1) the Iverson model (Iverson, 2000), Eq. (7), 2) the Harp model (Harp et al., 2006), Eq (8), 3) the Milledge model (Milledge et al., 2014) and, Eq (9), 4) the SLIP model (Montrasio, 2008; Montrasio and Valentino, 2016), Eq. (10). In slope stability analysis, the limit equilibrium method based on Mohr-Coulomb criterion is usually adopted to calculate slope stability. The one-dimensional theory considers the hypothesis of an infinitely extended slope characterized by soil thickness  $Z$  [m], plane inclination  $\alpha$  [°], saturated soil  $\gamma_s$  and water  $\gamma_w$  specific weight  $[kN m^{-3}]$ . The slope stability is evaluated by the Factor of Safety (FS), defined as the ratio between the resistant forces due to the friction and the mobilizing forces due to the weight component parallel to the slope. In CRHyME, the one-dimensional model was implemented by imagining each cell as a slope element for which the value of the safety factor FS is calculated. According to the principle of effective stress, as the soil moisture increases, normal efforts are reduced by an aliquot equal to the pressure generated by the water itself (Iverson, 2000).

$FS = \frac{\tan(\varphi)}{\tan(\alpha)} - \frac{\psi \gamma_w \tan(\varphi)}{\gamma_s Z \sin(\alpha) \cos(\alpha)} + \frac{c}{\gamma_s Z \sin(\alpha) \cos(\alpha)}$	(7)
$FS = \frac{\tan(\varphi)}{\tan(\alpha)} + \frac{m \gamma_w \tan(\varphi)}{\gamma_s \tan(\alpha)} + \frac{c}{\gamma_s Z \sin(\alpha)}$	(8)



$FS = \frac{2F_{rl} + F_{rb} + F_{rd} - F_{du}}{F_{dc}}$	(9)
$FS = \frac{N' \tan \varphi + C'}{W' \sin \alpha + F'}$	(10)

The key parameters of the Iverson (Iverson, 2000) Eq. (7) and Harp (Harp et al., 2006) models Eq. (8) are essentially 3: the friction angle  $\varphi$  [°] and the cohesion of the soil  $c$  [kPa] which are a function of the terrain granulometry, and the superficial soil moisture  $S_m(t)$  [m]. Inside Iverson's model is described by the groundwater pressure head of the local aquifer  $\psi = f(S_m(t))$ , expressed in [kPa], while inside the Harp model is described by the dimensionless variable  $m = \frac{h_{soilwater}(t)}{Z \cdot n}$ , comprised between 0 (completely dry) and 1 (completely wet). The Milledge model (Milledge et al., 2014) Eq. (9) considers not only the friction effects along the sliding surface  $F_{rb}$  expressed in [N], but also the shear resistance along the two parallel and vertical side walls  $F_{rl}$  in [N], the passive force of the upstream terrain  $F_{du}$ , in [N], the active force of the valley terrain  $F_{rd}$  in [N], and the mobilizing force due to the terrain weight  $F_{dc}$ , in [N]. In the SLIP model (Montrasio, 2008; Montrasio and Valentino, 2016) shown in Eq. (10) the terms are expressed in [N]:  $N'$  is the normal component of the weight as a function of porosity  $n$  and soil moisture  $S_m(t)$ ;  $C'$  is the cohesion term;  $W'$  is the slope parallel component of the weight as a function of porosity  $n$  and soil moisture  $S_m(t)$ ;  $F'$  is the term that expresses the seepage forces that are related to the presence of the temporary water table. Since slopes are vegetated, two other factors should be included: the additional cohesion of the root system of trees and the additional weight of plant biomass (Cislaghi et al., 2017; Yu et al., 2018; Rahardjo et al., 2014). As a matter of fact, in the absence of root cohesion, several slope areas would be perpetually in conditions of instability with  $FS < 1$ . The addition of root cohesion, varying between 1 – 10 kPa depending on the tree species and the type of land use was included in the stability evaluation (further details in Abbate and Mancusi, 2021a).

A debris flow represents movements of mass that are often triggered on steep slopes and travel long distances reaching the fan close to the watershed outlet (Takahashi, 2009). Debris flows are classified as landslides, although they are among the more fluid types of landslides (Iverson et al., 1997). Therefore, solid concentration within the saturated deposit and the presence of superficial water flowing above are the key parameters for assessing the triggering condition. As can be appreciated by Eq. (11) and (12), two criteria are at least to be included. The first one is derived from the theory of infinite slope stability where the solid concentration parameter  $C_*$  is included as the principal triggering factor. The solid concentration  $C_*$  is the grain concentration by volume in the static debris bed and can be expressed by the ratio between the soil amount [m<sup>3</sup>] to the sum of the soil amount [m<sup>3</sup>] and soil water volume [m<sup>3</sup>]. Increasing the local water volume, the solid concentration starts to progressively reduce. The first criterium in Eq. (11) requires the indication of soil density  $\sigma$  [kg m<sup>-3</sup>], water density  $\rho$  [kg m<sup>-3</sup>], the surface runoff height  $h_{runoff}$  [m] and the parameter  $a_{df}$  that can be assumed equal to the representative diameter of the soil deposit, such as  $D_{50}$ , expressed in [m]. The second criterium in Eq. (12) considers that specific superficial runoff discharge  $q_1 = \frac{F_{kin-dyn}(t)}{\Delta x}$ , in [m<sup>2</sup>s<sup>-1</sup>], flowing above the debris deposit, satisfies the threshold condition  $\geq 2$  for the non-dimensional water discharge  $q^*$  [-], where  $g$  is gravity acceleration [m s<sup>-2</sup>]. If these criteria are satisfied under a predetermined rainfall condition that basin could be subjected to debris flow triggering.

$FS_{debris} = \frac{\frac{C_*(\sigma - \rho)}{C_*(\sigma - \rho) + \rho \left(1 + \frac{h_{runoff}(t)}{a_{df}(D_{50})}\right)} \tan \varphi}{\tan(\alpha)}$	(11)
$q_* = q_i / \sqrt{D_{50}^3 * g} \geq 2$	(12)

### 2.2.3.2 Erosion production and bed-load solid transport routing

310 Gavrilovic's method (summarized in Eq. 13-14-15) is a semi-quantitative method capable of giving an estimation of erosion and sediment production in a basin (Longoni et al., 2016; Milanese et al., 2015; Globevnik et al., 2003; Brambilla et al., 2020). It was initially developed in southern ex-Yugoslavia and then successfully applied in Switzerland and Italy. The mean annual volume of eroded material  $G$ , expressed in  $[m^3 yr^{-1}]$ , is a product of  $W_s$  and  $R_{EPM}$ , which are respectively the mean annual production of sediment due to surface erosion, expressed in  $[m^3 yr^{-1}]$  Eq. (14), and the retention coefficient, adimensional

315  $[-]$  in Eq. (15) considers the possible re-sedimentation of the eroded material across the watershed.

$G = W_s R_{EPM}$	(13)
$W_s = \pi \bar{P} \tau_G(\bar{T}) \bar{Z}_{EPM}^3 A_{Basin} \rightarrow W_{s_{downscaled}} = \pi P(t) \tau_G(T(t)) Z_{EPM}^3(x, y) \Delta x \Delta y$	(14)
$R_{EPM} = \frac{\sqrt{OD}(l + l_{lat})}{(l + 10)A_{basin}}$	(15)

The terms that appear in the equations are  $\tau_G$  temperature coefficient  $[^\circ C]$  in function of watershed mean annual temperature  $\bar{T}$  in  $[^\circ C]$ ,  $\bar{P}$  mean annual precipitation value  $[mm yr^{-1}]$ ,  $\bar{Z}_{EPM}$  mean erosion coefficient  $[-]$ ,  $A_{basin}$  basin area  $[km^2]$ ,  $O$  perimeter of the basin  $[km]$ ,  $D$  mean elevation of the basin  $[km]$ ,  $l$  length of the main watercourse  $[km]$ ,  $l_{lat}$  the total length of the lateral tributaries  $[km]$ . The Gavrilovic method was developed to work with annual data of mean precipitation and temperature. Since with CRHyME we are interested in a continuous simulation, the method has been temporally and spatially downscaled (Eq. 14) by substituting  $\bar{P}$  and  $\bar{T}$  with the time-series of precipitation  $P(t)$   $[mm timestep^{-1}]$  and  $T(t)$  temperature  $[^\circ C]$  and calculated for each domain cell ( $A_{Basin} \rightarrow \Delta x \Delta y$ ). The values of  $Z_{EPM}$  are correlated to the land use characteristics and geological maps (Milanese et al., 2015; Abbate and Mancusi, 2021a) therefore the coefficient was spatially distributed through these parameters using the conversion relation proposed by (Globevnik et al., 2003).

325

The Gavrilovic method defines  $W_s$  as the source of available sediment that can be routed through the watershed until the outlet. In CRHyME the solid routing has been modelled considering its strong relation with liquid discharge. First of all, the theory of incipient motion of Shields that states the starting motion of sediments in the function of  $D_{50}$  quantity, the median diameter of the soil granulometric curve (Chow et al., 1988; Merritt et al., 2003; Vetsch et al., 2018), is implemented (Figure 4). The solid discharge is evaluated in two ways. A first calculation considers a stream-power formula for bed load transport (Morgan and Nearing, 2011; Shobe et al., 2017; Campforts et al., 2020). Here, the solid discharge  $Q_s$ , expressed in  $[m^3 s^{-1}]$ , is in function of the reach hydraulic and geometrical characteristics (Figure 4) and it doesn't consider the local availability of the eroded material in the channel that may decrease/increase the amount of sediment delivered. This first implementation of solid transport routing is also defined as Transport Limited (TL). A second calculation represents an adaptation of the kinematic model for clear water to the sediment transport, under the hypothesis that the velocity of sediment transport is assumed similar to the water flow. The application of the kinematic method requires the estimation of stage-discharge relations for the sediment in analogy with the clear water stage-discharge functions. Several authors (Govers, 1989; Govers et al., 1990; Rickenmann, 1999) have considered this hypothesis reasonable when no further additional information about solid transport is available. For this second case, the sediment balance is required and it has been assessed in each cell domain through Eq. (16) considering:

335

340 the erosion rate  $E_s$  equal to the source term  $W_s$  computed by Gavrilovic and the deposition rate  $D_s$  (Shobe et al., 2017), expressed in  $[m^3 yr^{-1}]$ ; the transport term  $T_s$  considering the kinematic model adapted for sediment routing, expressed in  $[m^3 s^{-1}]$ ; the sediment amount  $h_{solid}(t)$  in  $[m]$ , converted in volume  $[m^3]$  if multiplied by cell area extension  $[m^2]$ . This second implementation is representative of the Erosion Limited (EL) condition where the sediment availability in the river or on the slopes tends to limit effective water erosion, as it frequently happens (Shobe et al., 2017; Campforts et al., 2020; Chow et al., 1988; Davy and Lague, 2009).

345

$$\frac{dh_{solid}(t)}{dt} \cong \frac{\Delta h_{solid}(t)}{\Delta t} \pm \frac{T_s(t)}{\Delta x * \Delta y} = D_s(t) - E_s(t) \quad (16)$$

In CRHyME both TL and EL methods are evaluated for assessing quantitatively sediment transport yield within a physically reasonable range. According to Papini et al., 2017; Ivanov et al., 2020a; Dade and Friend, 1998a; Lamb and Venditti, 2016; Peirce et al., 2019; Pearson et al., 2017; Ancey, 2020, the sediment transport dynamic is an active research frontier. In this sense, the spatial distribution of  $D_{50}$  is a critical point because is difficult to be reconstructed at the catchment scale (Abeshu et al., 2021). Moreover,  $D_{50}$  distribution influences incipient motion threshold that sensibly modifies the local sediment routing leading to wrong estimations of the watershed sediment yield. Since it doesn't exist a close formulation for indirectly estimating the granulometry in the absence of an on-field survey dataset, empirical approaches have been proposed by (Nino, 2002; Sambrook Smith and Ferguson, 1995; Lamb and Venditti, 2016; Berg, 1995). According to these authors, several morphological, climatic, hydrological, and geological factors can influence river granulometry in a particular section. Among them, slope-like factors have shown a quite significant correlation with  $D_{50}$  and in some cases slope  $\rightarrow D_{50}$  relations (power-laws in the form like  $D_{50} = a_x Slope^{bx}$ ) were retrieved (Nino, 2002). Namely,  $D_{50}$  tends to increase with slope steepness. These relations mimic the formula proposed by Berg, 1995 where the  $D_{50}$  is indirectly determined using a power-law function describing the river morphology evolution. Even though slope  $\rightarrow D_{50}$  represent a crude approximation it has a physical meaning since in the upper catchment (where slopes are steepness) coarse granulometries are generally prevalent while at the outlet (where slopes are lower) the sediment fine fraction becomes more significant (Tangi et al., 2019). In CRHyME, the  $D_{50}$  is a necessary granulometric data, therefore an ensemble of empirical slope  $\rightarrow D_{50}$  curves have been included to assess automatically  $D_{50}$  distribution across the catchment using the slope data. Curve's parameters were calibrated ad hoc in the examined areas comparing simulated sediment yields to the available measurements and with on-site granulometry surveys conducted.

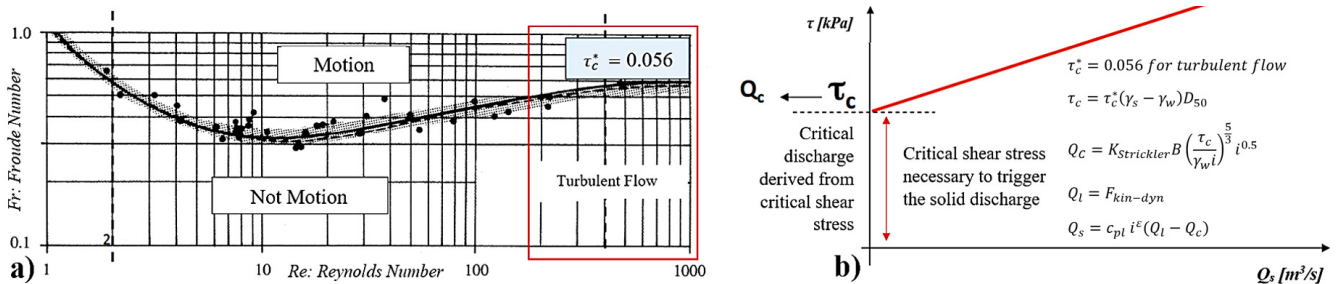


**Figure 4:** a) Shield abacus (Chow et al., 1988) for solid transport incipient motion under different conditions of turbulence (Re number) and flow regime (Fr number). In the red box is defined the typical range of turbulent flow in rivers with a critical dimensionless shear stress  $\tau_c^*$  of 0.056; b) evaluation of the incipient motion condition for solid transport discharge  $Q_s$  using power-law relation where: the critical shear stress  $\tau_c$  [kPa] and the critical liquid discharge  $Q_c$  [ $m^3 s^{-1}$ ] are a function of saturated grain  $\gamma_s$  and  $\gamma_w$  and water specific weights [ $kN m^{-3}$ ], the local granulometry through the parameter  $D_{50}$  [mm], the roughness  $K_{Strickler}$  [-], the channel width  $B$  [m], the reach slope  $i$  [%] and the two coefficients  $\epsilon$  [-] (comprised between 1 and 2) and  $c_{pl}$  [-] (comprised 0.94 and 5.8) (Vetsch et al., 2018).

### 2.2.3.3 Connections within geo-hydrological processes

The processes here described may occur simultaneously inside a catchment, especially during heavy rains or after periods of prolonged precipitation (Abbate et al., 2021a). In CRHyME, the erosion and sediment transport are well integrated within the hydrological routines following the state-of-the-art in the literature (Vetsch et al., 2018). Here, both the triggering function (sediment detachment and incipient motion) and the magnitude (amount of sediment eroded and transported) have been quantified. On the other side, for shallow landslide and debris flow, only the triggering condition of failure has been analysed while the mass wasting propagation across the catchment has not been included in the code yet. This choice is motivated by the fact that mass wasting failures, especially for debris flows, are characterized by large uncertainties in their volume

quantification related mainly to the entrainment processes and their runoff strongly depends on DTM accuracy and spatial resolution (i.e. they are spatial scale dependent) (Jakob and Hungr, 2005; Scheidl and Rickenmann, 2011). The entrainment effect is difficult to be modelled in a closed form and it may perturb the volume estimation by orders of magnitude (D'Agostino and Marchi, 2001). Mass wasting processes may have a strong incidence on sediment transport dynamic and compared to widespread erosion, which is a "low intensity" process, landslides may change abruptly the geo-morphological characteristics of the catchment (Iida, 1999; D'Odorico and Fagherazzi, 2003). These issues are under study, but preliminary results are not investigated in this present work.

## 2.3 Model performance

### 2.3.1 Hydrological indexes and sediment transport assessment

Assessing hydrological performance at basin outlets is evaluated through error indexes that compare water discharges recorded by the local hydrometer and the water discharge simulated by the model (Chow et al., 1988; Bancheri et al., 2020). The most common indexes are the Nash–Sutcliffe Efficiency (NSE), and the Root-Mean-Square Error (RMSE). The Nash–Sutcliffe Efficiency (NSE) in Eq. (17) is a normalized model efficiency coefficient where  $S_i$  and  $M_i$  are respectively the predicted (or simulated) and measured (or observed) values at a given time step  $i$ . The NSE varies from  $-\infty$  to 1, where 1 corresponds to the maximum agreement between predicted and observed values. The Root-Mean-Square Error (RMSE) in Eq. (18) is given by where  $S_i$  and  $M_i$  are respectively the predicted (or simulated) and measured (or observed) time series, and  $N$  is the number of components in the series.

$NSE = 1 - \frac{\sum_{i=1}^n (S_i - M_i)^2}{\sum_{i=1}^n (M_i - \bar{M}_i)^2}$	(17)
$RMSE = \sqrt{\frac{1}{N} \sum_{i=1}^n (M_i - S_i)^2}$	(18)

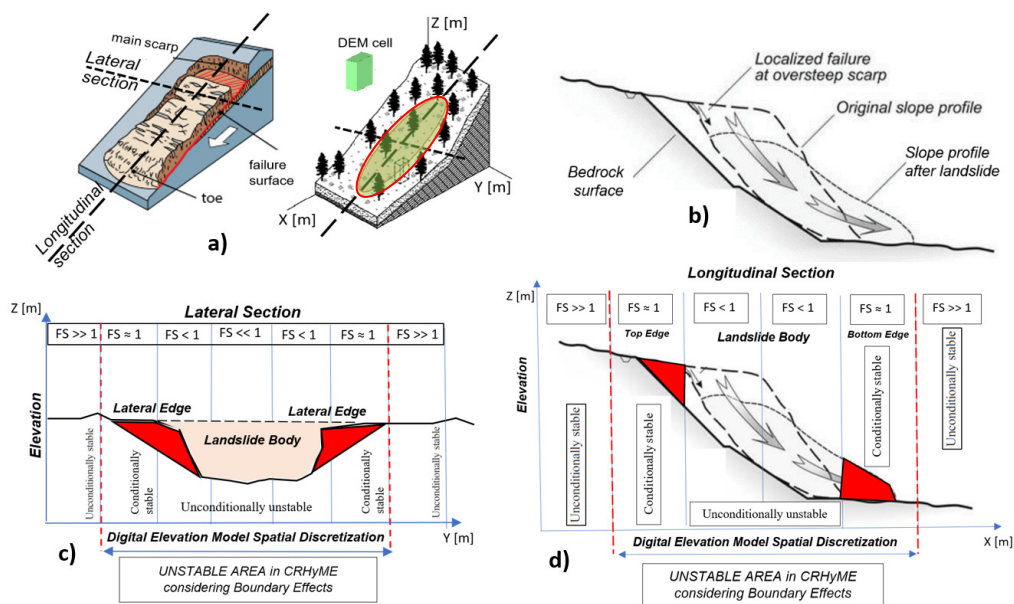
For the sediment transport assessment, the periodical bathymetry campaigns carried out inside hydropower reservoirs can be considered as a reference (Pacina et al., 2020; Langland, 2009; Marnezy, 2008) of the sediment yield measurement. Compared to hydrometric data which can be easily gathered from local environmental agencies (Rete Monitoraggio ARPA Lombardia; Rete Monitoraggio ARPA Emilia), bathymetries are generally not accessible to the public (ITCOLD, 2009, 2016). Therefore, the calibration and validation of erosion and sediment transport models have considered the seasonal volume estimation in hydropower reservoirs and the event-based volume estimation only where available. For the case studies analysed, these data were retrieved also from specific reports (Milanesi et al., 2015; Ballio et al., 2010; Brambilla et al., 2020).

### 2.3.2 ROC curves for local landslide prediction

According to several authors (Formetta et al., 2016; Pereira et al., 2016; Vakhshoori and Zare, 2018; Gudiyangada Nachappa et al., 2019; Kadavi et al., 2018; Fawcett, 2006), a useful technique to assess the prediction performances of a slope stability model is the Receiver Operating Characteristic (ROC) methodology. The ROC curve illustrates the diagnostic ability of a binary classifier system as its discrimination threshold is varied. In landslide stability assessment, the binary classificatory is the condition of  $FS \geq 1$  (stable) or  $FS < 1$  (unstable) characterizing each pixel of the model domain (Formetta et al., 2016; Vakhshoori and Zare, 2018). In CRHyME, the number of landslide activations is counted. On each timestep, a 0-1 map is produced where the destabilized pixels ( $FS < 1$ ) are signed as 1 while stable pixels ( $FS \geq 1$ ) are signed with 0. This landslide-triggering algorithm is rather simple to be implemented inside a code and other authors have also followed this approach (Harp et al., 2006; Milledge et al., 2014; Formetta et al., 2016). However, in our opinion, the inclusion of a "pixel-buffer" in the surrender area of a detected unstable pixel (prone to shallow landslide failure) is necessary to describe more physically the instability activation. Generally speaking, landslide instability areas are not confined to the landslide body but could extend to

surrounding boundaries: in the upper part, the landslide crown could experiment with further collapse since other cracks may generate and propagate retrogressively (Ivanov et al., 2020b); in the bottom part, the landslide may evolve into soil slip or earth flow and travel along the slope following the maximum gradient (Jakob and Hungr, 2005); the lateral boundaries could be also affected by landslide instability due to shear stress perturbation and reduced lateral roots cohesion (Rahardjo et al., 2014) that develops during landslide collapsing. Bearing in mind that a single-pixel slope failure evaluation may be not conservative from a hazard perspective, in CRHyME the unstable area related to the predicted unstable pixel has been extended considering also the surrounded 8 adjacent cells, as reported in Figure 6.a.

A 9-pixel counting may overestimate in some cases the extension of the hazardous area because it is also dependent on the DTM resolution. To assure the reasonability of this choice, a survey conducted within the IFFI (Inventario Fenomeni Franosi Italiano) landslide inventory (ISPRA, 2018; Guadagno et al., 2003; Guzzetti and Tonelli, 2004) has shown that typical rainfall-induced shallow landslides have mean and median spatial extension equal to  $\sim 20'000 \text{ m}^2$  and  $\sim 10'000 \text{ m}^2$  respectively, which correspond an indicative pixel size comprised between 150 – 100 m. In our case, the 90 m DTM resolution (sampled at the equator) becomes  $\sim 70 \text{ m}$  at the latitude of the tested case study due to geographical transformation (Lehner et al., 2008). Therefore, a 9-pixel approximation could bring the overall landslide extension equal to  $(70 \times 3)^2 \sim 40'000 \text{ m}^2$ , slightly larger compared to the inventory range but within the same order of magnitude calculated from the IFFI inventory. However, the exact landslide geometry is not definable “a priori” since it has large variability in terms of extension and shape (areas span mostly  $10^3$  to  $10^6 \text{ m}^2$  according to Tanyaş et al., 2019) which could be larger or narrower compared to DTM resolution (Figures 5.a and 5.c). Moreover, Oguz et al., 2022, Zheng et al., 2020, Legorreta Paulin et al., 2010, Michel et al., 2014 have shown how DTM resolution and its accuracy may significantly perturb the local stability at the top and bottom edges, extending or reducing the effective unstable slopes (Figures 5.b and 5.d). According to Legorreta Paulin et al., 2010 a higher DTM resolution could improve the unstable area description reducing size over/underestimation but it would increase sensibly the computational cost of the hydrological model (Zhang et al., 2016). These issues will be further discussed in section 4.4.



440 **Figure 5: Scale dependence in the infinite slope stability assessment. a) geometrical sections (longitudinal and lateral) of shallow landslides, b) landslide kinematics along longitudinal section, c) exemplification of stable and unstable areas in lateral section, d) exemplification of stable and unstable areas in longitudinal section with respect to DTM resolution. In red are highlighted the lateral, top and bottom edges of the landslide affected by instabilities.**

445 Since the reference data on historical landslides in the IFFI inventory comes from several sources, the localization of the shallow instability could not be georeferenced geo-localized with high precision, especially for historical events where sometimes only triggering point locations (not the landslide polygon) are reported (ISPRA, 2018). To carry out the ROC methodology and avoid reference data issues, a buffer zone with different radii around each landslide point was created: 250

m, 500 m, 1000 m and 2000 m (Figure 6). This radius represents an attempt to cope with the uncertainties about the real  
 450 position and extension of the triggered landslide.

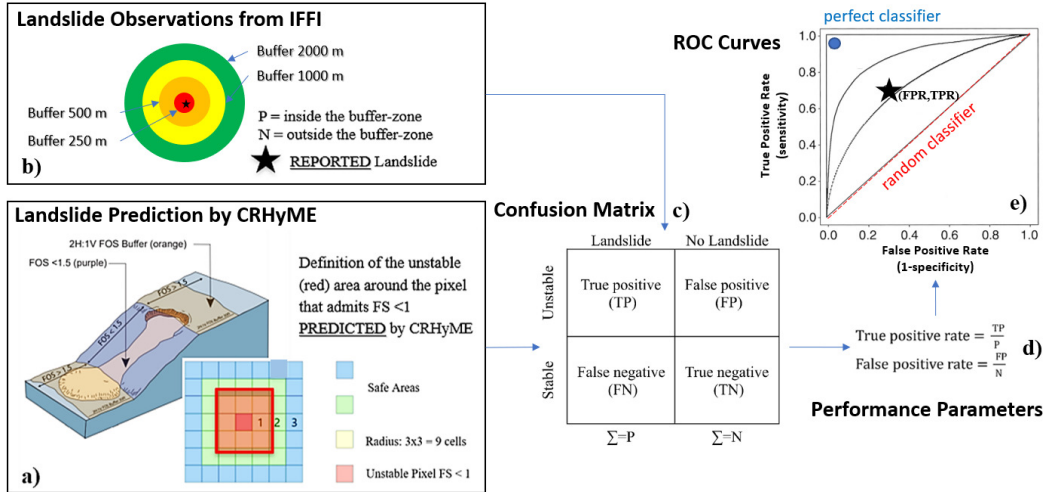


**Figure 6: ROC methodology scheme to assess the CRHyME model performances in detecting landslide failures that occurred after a rainfall event. a) unstable areas predicted by CRHyME considering the surrounded 8 cells, b) unstable area reported in IFFI considering buffer-zones due to geo-localization uncertainties, c) confusion matrix and parameters TP, FN, TN and FP calculation, d) evaluation of performance parameters TPR and FPR for the graphical representation of the ROC curves d).**

Knowing the observed and the predicted instabilities (retrieved by IFFI and simulated by CRHyME) referring to a specific  
 geo-hydrological event, the ROC assessment was conducted. The ROC curves were built following the scheme presented in  
 Figure 6. Through a confusion matrix (Figure 6.c), the False Positive Rate (1-specificity, FPR) Eq. (19) and the True Positive  
 460 Rate (sensitivity, TPR) Eq. (20) are calculated (Figure 6.d), and the point (FPR, TPR) is reported in the ROC graph (Figure  
 6.e). The upper left corner of the graph (TPR = 1 and FPR = 0) represents the perfect performance (or perfect classifier), and  
 the diagonal line, represents the random classification or “no skill”. As the point (FPR, TPR, the prediction skill) plotted on  
 the ROC graph is closer to the upper left, the prediction capacity of the CRHyME model is better.

$FPR = \frac{FP}{N} = \frac{FP}{FP + TN}$	(19)
$TPR = \frac{TP}{P} = \frac{TP}{TP + FN}$	(20)

## 465 2.4 Cases studied

The cases of study considered for CRHyME simulations are located in Northern Italy and are here presented (Figure 7).  
 The Caldane basin (Figure 7.a) represents the on-field laboratory of the University of Politecnico di Milano (Brambilla et al.,  
 2020). The basin is about 27 km<sup>2</sup> situated near the city of Lecco (Lombardy region) across the Pre-Alps and is characterized  
 by intense sediment transport. The catchment is well monitored by 5 rain gauge stations, a hydrometer at the outlet and two  
 470 sediment check-dams where the sediment yield is constantly monitored with periodic bathymetric surveys. The lithology of  
 the area is constituted by consolidated calcareous rocks with good strength properties but rather susceptible to rainfall erosivity.  
 Karst is present in the surrounding region but is not relevant in the Caldane catchment (Papini et al., 2017). From a climatic  
 viewpoint, the area has a mean precipitation of 2000 mm yr<sup>-1</sup> (Rete Monitoraggio ARPA Lombardia).  
 The Valtellina valley (Figure 7.b) is settled in the northern part of the Lombardy region across the Central Alps and in 1987  
 475 experienced a dramatic geo-hydrological episode triggered by rather intense and prolonged rainfalls. The effects on the  
 territory were severe: shallow landslides, debris flows, and flash floods were recorded causing human injuries and fatalities  
 and extensive damage to infrastructure and buildings (Luino, 2005). The secondary branch of Mallerio River also experienced

intense sediment transport during the 1987 flood, which affected Sondrio town. Similar events iteratively hit the area in November 2000 and 2002. The Valtellina valley has E-W topographical development, and its geomorphology is characterized by a strong difference between the opposite slopes. In the southern flank of the valley, the Orobic Pre-Alps are constituted by consolidated metamorphic rocks (Gneiss) while across the Retiche Alps (northern flank), magmatic and sedimentary rocks alternate with metamorphic. The most prevalent type of soil texture is formed by sandy loam and silty loam (Crosta and Frattini, 2003; Longoni et al., 2016). The valley is characterized by a strong precipitation variability in the range of a minimum of 600 mm yr<sup>-1</sup> in the north-eastern part of the Retiche Alps and a maximum of 3500 mm yr<sup>-1</sup> in the south-western sector of the Orobic Pre-Alps (Rete Monitoraggio ARPA Lombardia). According to this, two different meteorological datasets were examined here to test the ability of CRHyME to deal with different rainfall datasets. The first one has considered the meteorological data provided by the Regional Agencies for Environmental Protection (ARPA Lombardia) (Rete Monitoraggio ARPA Lombardia) ground-based weather stations. The second one is MERIDA, the MEteorological Reanalysis Italian Dataset (Bonanno et al., 2019). MERIDA consists of a dynamical downscaling of the new European Centre for Medium-range Weather Forecasts (ECMWF) global reanalysis ERA5 using the Weather Research and Forecasting (WRF) model, which is configured to describe the typical weather conditions of Italy.

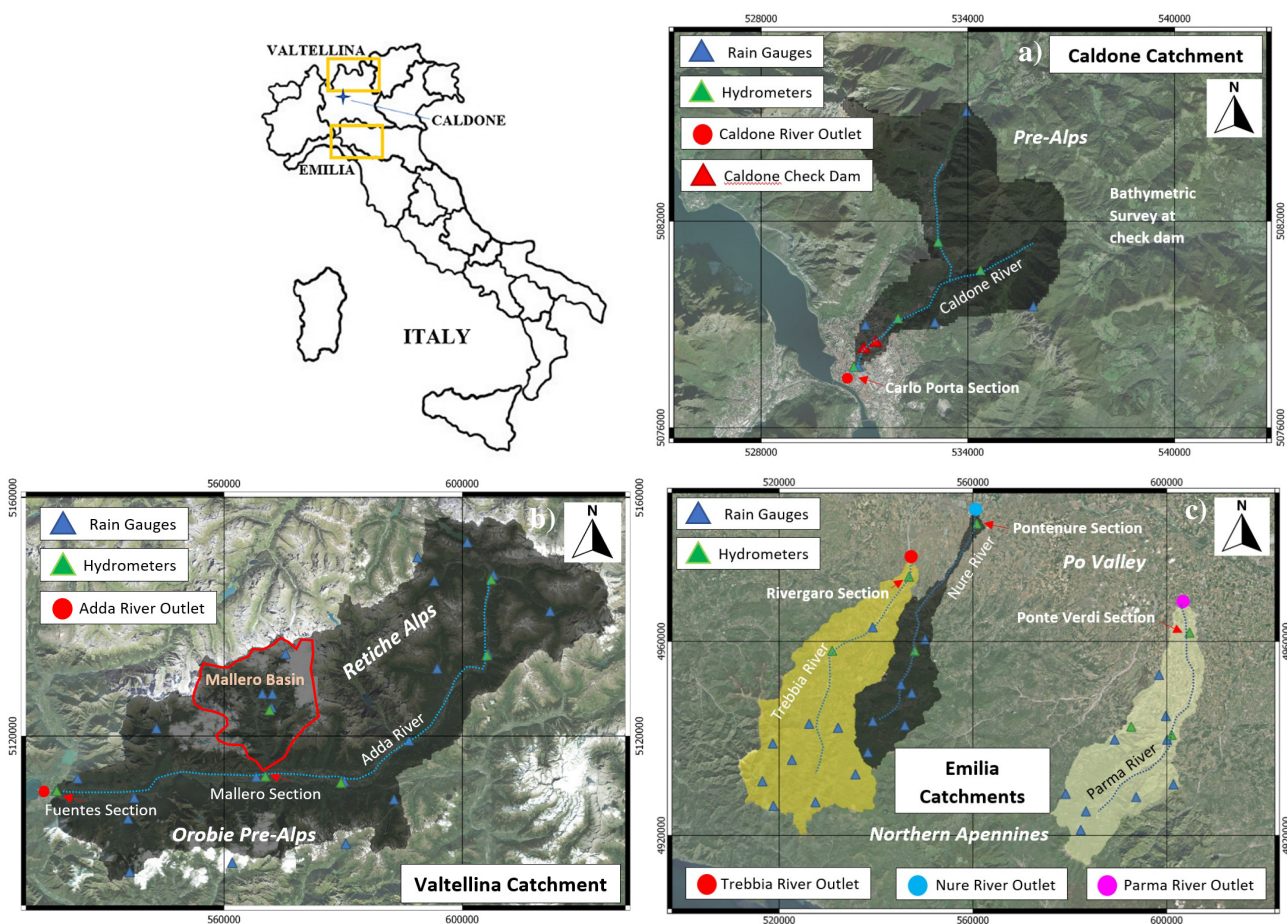


**Figure 7: The Caldone a), the Valtellina b) and the Emilia c) catchments studied. Rain gauges, hydrometer stations and river outlets are indicated in a), b), c). Hydrometric stations considered for assessing the CRHyME performances are located at Carlo Porta section (for the Caldone River), Fuentes and Mallerio sections (for the Adda and the Mallerio Rivers) in the Valtellina catchment, and Rivergaro (for Trebbia River), Pontenure (for Nure River) and Ponte Verdi (for Parma River) sections across the Emilia. Base layer from © Google Maps 2023.**

The Emilia area is situated in the Northern Apennines (Figure 7.c) and experienced intense geo-hydrological episodes in October 2014 and September 2015 (Ciccarese et al., 2020). Three watersheds were particularly affected: the Trebbia, Nure and Parma catchments. The event of October 2014 mainly hit the Parma catchment while the event of September 2015 hit the Trebbia and Nure catchments. From a geomorphological viewpoint, the Northern Apennines represent a fold-and-thrust mountain chain where several landslide instabilities are present due to the post-failure weathering of claystone, sandstone, and

limestone rock fragments. These deposits are in residual strength conditions and can be quite easily mobilised and trigger  
505 debris flows during heavy rain episodes (Parenti et al., 2023). The Emilia region is characterized by a rainfall distribution with  
a south-north gradient where a maximum amount of 2000 mm yr<sup>-1</sup> is recorded in the highest relief of the Apennines (south)  
while the 700 mm yr<sup>-1</sup> characterizes the floodplain areas of the Po Valley in the northern part (Rete Monitoraggio ARPA  
Emilia).

During the CRHyME calibration and validation procedure, monitoring points for checking the water discharge and volume  
510 were chosen in correspondence with the reference hydrometers located at the catchment outlets (green triangles in Figures  
7.a,b,c). Check dams and hydropower reservoirs were considered for estimating reference sediment yield: a check dam close  
to the outlet for the Caldone catchment (red triangles in Figure 7.a), three hydropower reservoirs of Campo Tartano, Valgrosina  
and Cancano for the Valtellina case study (red triangles in Figure 10.a) and AdBPo reference data (Autorità di Bacino  
Distrettuale del Fiume Po, 2022) for the Emilia case study. Regarding shallow landslides and debris flows, a literature survey  
515 has been conducted within the IFFI inventory to find an available inventory of the failures (Figures 11.a and 13.a) that occurred  
during the past geo-hydrological events simulated.

### 3 Results

#### 3.1 Caldone case study

The Caldone catchment was investigated to verify the numerical conservativity of hydrological and sediment balance  
520 calculated by CRHyME, to explore the sensitivity to the variation of spatial resolution of the input data (e.g. DTM) and to  
calibrate and validate the slope → D<sub>50</sub> empirical relations. According to Rocha et al., 2020; Tavares da Costa et al., 2019), a  
spatially distributed hydrological model is sensitive to input data resolution. The reconstruction of the catchment parameters,  
such as the flow accumulation and the flow direction, depends on the characteristics of the DTM. As a result, routing methods,  
which depend on the flow direction, may experience differences in results under different cell resolutions. Moreover,  
525 increasing the DTM resolution is generally time-consuming due to the large number of cells within the computational domain.  
To test these aspects in CRHyME, for the Caldone catchment were executed four runs in a short period of 6 months, considering  
four different DTM resolutions: 90 m, 50 m, 20 m and 5 m. In Table 2 the simulation settings are resumed. To initialize  
CRHyME, the meteorological data series were gathered from the ARPA Lombardia agency (Rete Monitoraggio ARPA  
Lombardia) (Figure 6.a). The hydrometers data and the local stage-discharge relation were retrieved from the Lecco  
530 municipality station located at Via Carlo Porta (Figure 7.a). The rain gauges were spatially interpolated using the IDW  
technique (Chow et al., 1988) with a temporal resolution of 1 day. As can be appreciated from Table 2, the model's ability into  
the reproduction of a realistic water discharge tends to degrade progressively using a higher resolution. Looking at NSE scores  
for the discharge, the best accordance with the reference is reached in correspondence of a 50 m resolution. RMSE for the  
discharge is lower for a 50 m simulation. The model is conservative since the NSE for the volume is close to 0.8, verifying  
535 that almost all the precipitation volume has arrived at the outlet within the simulated period. The NSE for the volume is a  
parameter that is rather invariant with respect to the resolution while the NSE for the discharge is spatial scale dependent.

The influence of the slope → D<sub>50</sub> curves parameterization was the second aspect investigated in the Caldone catchment. A  
long-term simulation has been carried out from 1 January 2019 up to 31 December 2021 (Figure 8.a), with a DTM resolution  
of 50 m and after a “spin-up” period of 2 years for raising the model to realistic initial conditions. Considering the limited  
540 extension of the watershed, this period has revealed sufficient for assessing the performance of solid discharge. The sediment  
discharge was computed considering both TL (Transport Limited) and EL (Erosion Limited) options.

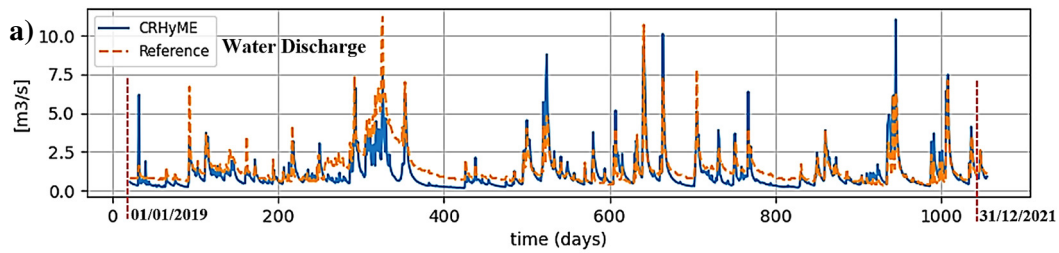
In Figure 8.b can be noticed that NSE for water discharge and volume exhibit a rather high score, about 0.462 and 0.719  
respectively. The former states that the reproduction of the hydrological part has been assessed almost correctly by CRHyME.  
Four slope → D<sub>50</sub> functions have been tested in the form like  $D_{50} = a_x \text{Slope}^{b_x}$  (Table 3): set 1, set 2, set 3 and set 4. Results



545 have shown that the choice of slope  $\rightarrow D_{50}$  can sensibly modify the outlet's sediment yield: the cumulated sediment amount increases with a decrease in the mean diameter. These data were compared with the onsite bathymetric surveys that were carried out 4 times across the investigated period Table 4. From the bathymetry measurements, a sediment yield of about  $1000 \text{ m}^3 \text{ yr}^{-1}$  was considered representative of Caldane River. In our sensitivity analysis, this value has matched the reference using set 2:  $2993 \text{ m}^3$  for 1055 days  $\approx 3$  yrs correspond to  $\approx 1000 \text{ m}^3 \text{ yr}^{-1}$ . Set n° 2 is slightly higher than the functions considered for Valtellina and Emilia simulations that are better represented by set n° 3.

Simulation Settings and Error Analysis	Simulation 1	Simulation 2	Simulation 3	Simulation 4
Spatial Resolution	90 m	50 m	20 m	5 m
Starting Date	01/05/2020	01/06/2020	01/06/2020	01/06/2020
Ending Date	10/10/2020	10/10/2020	10/10/2020	10/10/2020
Initial Soil Moisture	90%	90%	90%	90%
NSE (Volume) [-]	0.765	0.777	0.777	0.656
NSE (Discharge) [-]	0.341	0.650	-1.333	-2.610
RMSE (Discharge) [ $\text{m}^3 \text{ s}^{-1}$ ]	1.605	0.699	1.804	2.244

Table 2: Setting properties adopted for the Caldane River simulations and hydrological indexes ranking of volume and discharge testing different spatial resolutions of the DTM.



b)	NSE (Discharge)	NSE (Volume)	RMSE (Discharge) [ $\text{m}^3 \text{ s}^{-1}$ ]
Error Analysis	0.462	0.719	0.900

Figure 8: Hydrological simulation carried out for sediment transport assessment in the Caldane catchment with 50 m DTM resolution from 01/01/2019 up to 31/12/2021: a) simulated water discharge (blue line) vs. reference hydrometer at the Carlo Porta section (orange line) and b) hydrological indexes ranking of volume and discharge.

Curve Set	$a_x$ parameter	$b_x$ parameter	Slope $\rightarrow D_{50}$ Equations	Total Sediment Volume [ $\text{m}^3$ ]
Set 1	5604.8	2.38	$D_{50} = 5604.8 \text{ Slope}^{2.38}$	2608
Set 2	1786.9	1.79	$D_{50} = 1786.9 \text{ Slope}^{1.79}$	2993
Set 3	1453.1	1.61	$D_{50} = 1453.1 \text{ Slope}^{1.61}$	5947
Set 4	285.3	0.8	$D_{50} = 285.3 \text{ Slope}^{0.80}$	16446

560 Table 3: Slope  $\rightarrow D_{50}$  functions tested in the Caldane catchment, and the volume of the total sediment simulated by CRHyME at the basin outlet.

Bathymetry survey	Total Sediment Volume [ $\text{m}^3$ ]
20 July 2019 - 20 July 2020	$\approx 294$
20 July 2020 - 13 October 2020	$\approx 438$
13 October 2020 - 15 November 2021	$\approx 800$

Table 4: Bathymetric survey and total volume stored at the check dam close to the Caldane catchment outlet.

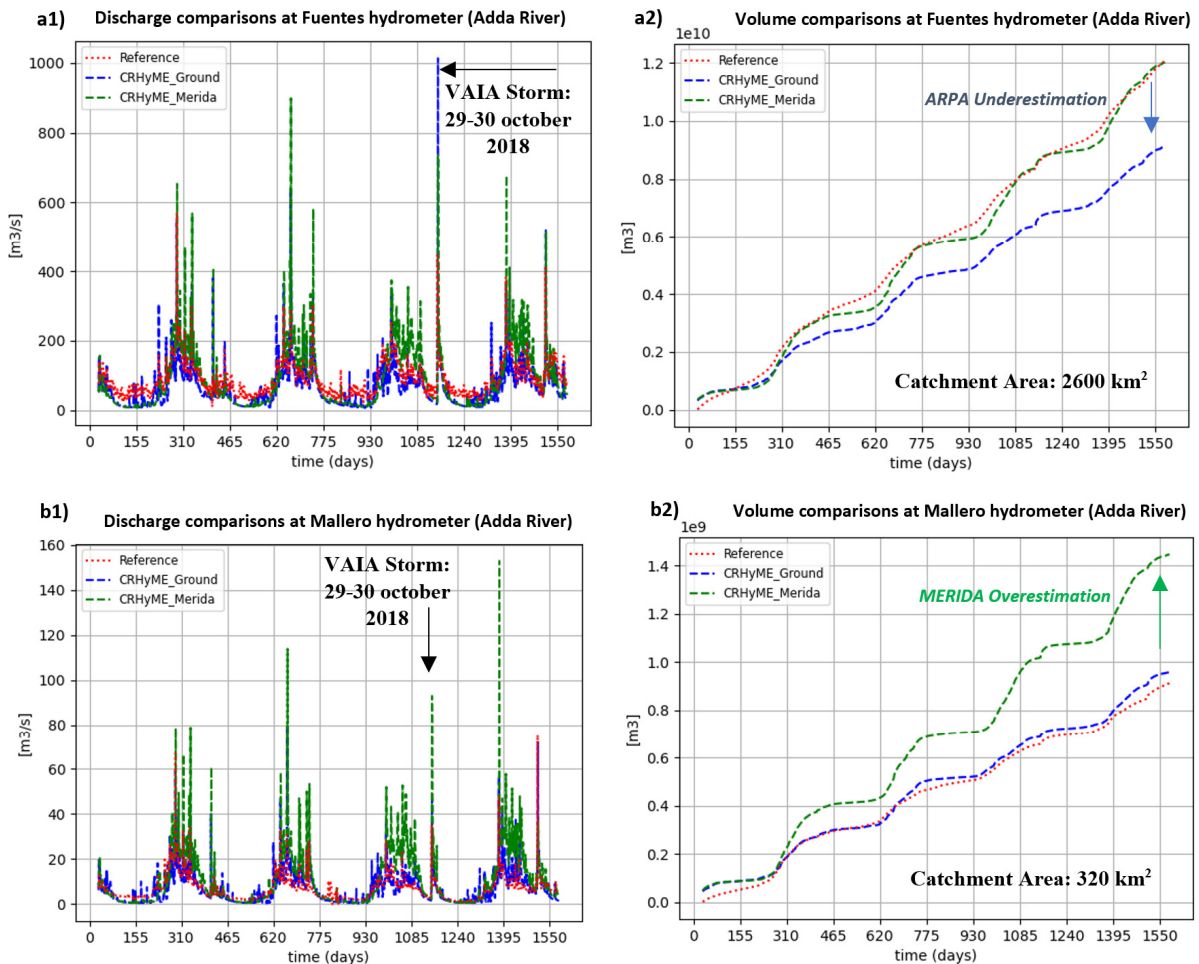
### 3.2 Valtellina case study

565 The analysis conducted for the Valtellina area has followed the steps reported in Table 5. The CRHyME calibration was carried out for three years between 1 September 2015 and 31 August 2018 after a “spin-up” period of 2 years for acquiring realistic initial conditions. Then, a subsequent validation period started on 1 September 2018 up to 31 December 2019. In Figure 9 the water discharges and the total volumes computed by CRHyME in the two reference sections of Fuentes (basin area = 2600 km<sup>2</sup>) and Mallero (basin area = 320 km<sup>2</sup>) are reported.

570

Settings for Valtellina catchment	Geo-Hydrological Event Simulated	Starting Date	Ending Date	Rainfall Dataset used
Calibration	-	01/09/2015	31/08/2018	ARPA Lombardia and MERIDA
Validation	October 2018	01/09/2018	31/12/2019	ARPA Lombardia and MERIDA
Validation	July 1987	01/09/1984	31/07/1987	ARPA Lombardia
Validation	November 2000	01/09/1997	30/11/2000	ARPA Lombardia
Validation	November 2002	01/12/2000	31/12/2002	ARPA Lombardia

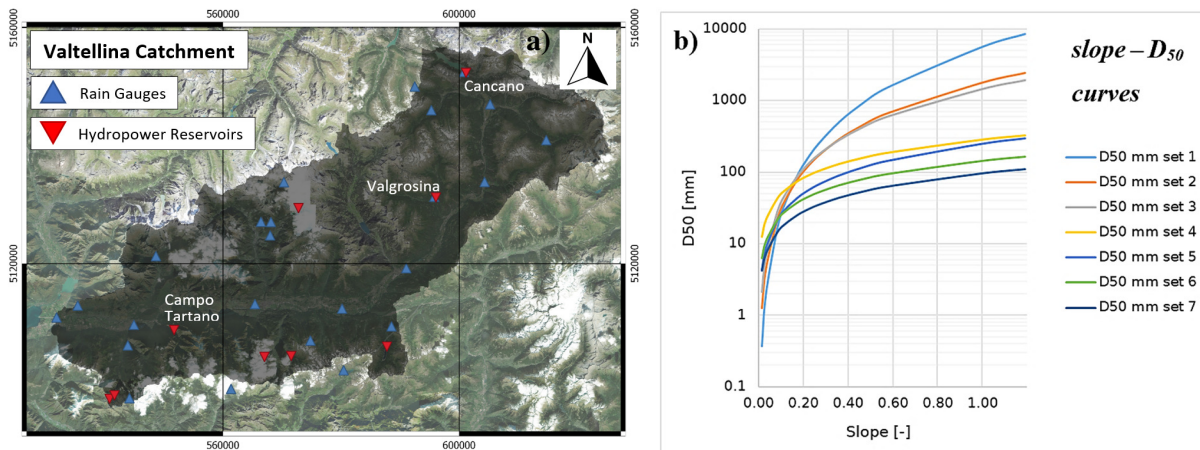
**Table 5: Simulation settings of the Valtellina case study. The calibration and validation of the model have considered more than 4 years of data on a daily basis gathered from ARPA Lombardia (Environmental Agency) weather stations and the MERIDA reanalysis database (Bonanno et al., 2019). These event-based simulations were carried out for significant geo-hydrological events of July 1987, November 2000, November 2002 and October 2018.**



575

Error Analysis of Hydrological Variables	NSE [-]	RMSE [ $\text{m}^3 \text{s}^{-1}$ ]	NSE_MERIDA [-]	RMSE_MERIDA [ $\text{m}^3 \text{s}^{-1}$ ]
Discharge Fuentes (Adda River)	0.199	45.370	-0.603	64.172
Volume Fuentes (Adda River)	0.783	-	0.993	-
Discharge Mallero (Adda River)	0.325	4.695	-2.369	10.494
Volume Mallero (Adda River)	0.988	-	-0.145	-

580 **Figure 9:** CRHyME model simulation results of water discharges (a1 and b1) and volume (a2 and b2) at the Fuentes (a), and the  
585 **Mallero (b) hydrometers** for the period 2015-2019 and using ARPA weather stations and MERIDA dataset. As can be appreciated,  
**the Volume performances are better than Discharge performances: the Valtellina basin is strongly regulated by hydropower plants and dams that operate a consistent lamination of the peak discharge during major rainfall events; the kinematic routing may be not sufficiently accurate for flood propagation across the valley floodplain since dynamic lamination may occur. As a result, green and blue spikes overestimate the peak discharge compared to the reference. The geo-hydrological event that occurred in late October 2018 (The Vaia Storm (Davolio et al., 2020)) has been recognized by CRHyME as one of the most intense, especially at the Fuentes section.**



c)

Curve Set	$a_x$ parameter	$b_x$ parameter	Slope $\rightarrow$ $D_{50}$ Equations	Literature Reference and Curve Calibration
Set 1	5604.8	2.38	$D_{50} = 5604.8 \text{ Slope}^{2.38}$	From (Berg, 1995), $b_x = 2.38$
Set 2	1786.9	1.79	$D_{50} = 1786.9 \text{ Slope}^{1.79}$	Decreasing $a_x$ and $b_x$
Set 3	1453.1	1.61	$D_{50} = 1453.1 \text{ Slope}^{1.61}$	Decreasing $a_x$ and $b_x$
Set 4	285.3	0.8	$D_{50} = 285.3 \text{ Slope}^{0.80}$	Decreasing $a_x$
Set 5	246.7	0.8	$D_{50} = 246.7 \text{ Slope}^{0.80}$	Decreasing $a_x$
Set 6	142.6	0.8	$D_{50} = 142.6 \text{ Slope}^{0.80}$	From (Nino, 2002), $b_x = 0.8$
Set 7	95.1	0.8	$D_{50} = 95.1 \text{ Slope}^{0.80}$	Decreasing $a_x$

d)

Sediment Yield Error Analysis	Campo Tartano Dam	Valgrosina Dam	Cancano Dam
Literature Reference	38'037 $\text{m}^3 \text{ yr}^{-1}$	33'600 $\text{m}^3 \text{ yr}^{-1}$	21'450 $\text{m}^3 \text{ yr}^{-1}$
Simulated 2015-2019	33'604 $\text{m}^3 \text{ yr}^{-1}$	34'324 $\text{m}^3 \text{ yr}^{-1}$	18'893 $\text{m}^3 \text{ yr}^{-1}$
% difference	-11.7 %	+2.15 %	-11.9 %

590 **Figure 10:** a) Valtellina case study area where hydropower reservoirs of Campo Tartano, Valgrosina and Cancano are indicated; b)  
and c) **Slope  $\rightarrow$   $D_{50}$  relations tested and implemented in CRHyME based on the theory of (Berg, 1995; Nino, 2002) and considering on-site surveys; d) Sediment yield estimations for the three dams of Campo Tartano, Valgrosina and Cancano where can be noticed the correct estimation with respect to the ITCOLD reference (ITCOLD, 2009, 2016). Base layer from © Google Maps 2023.**

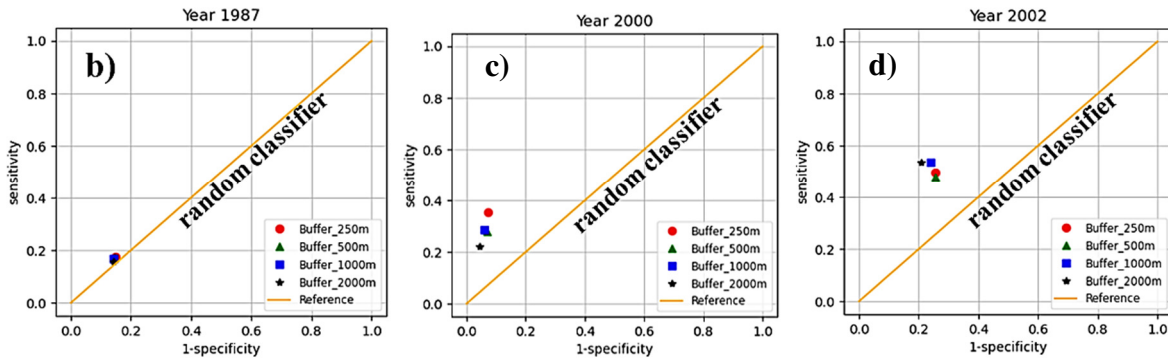
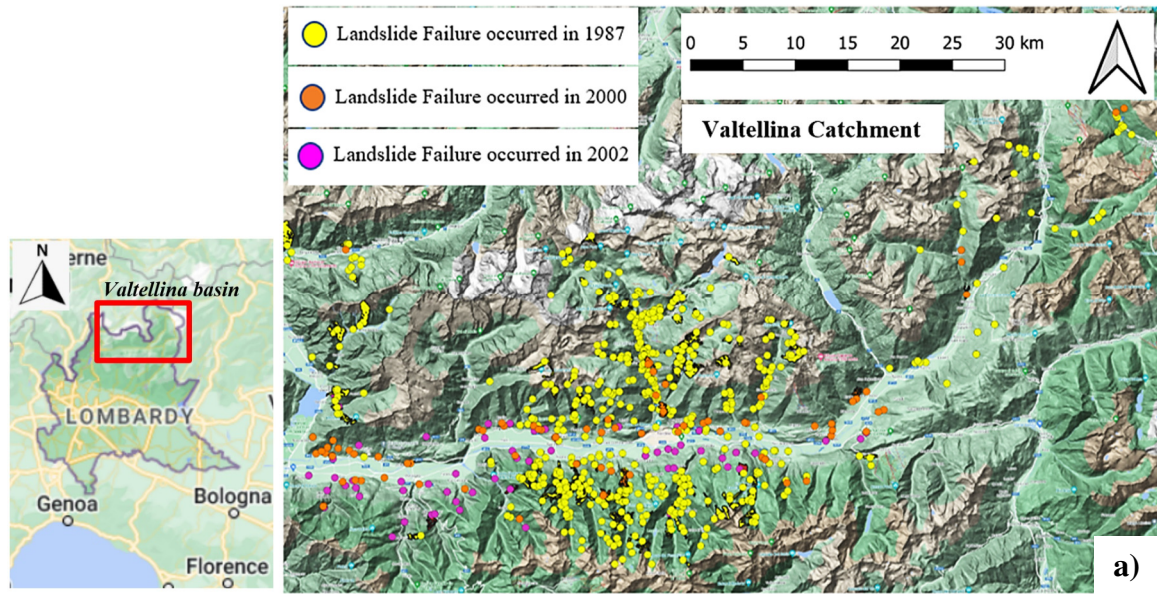
595 Looking at the simulation driven by the ARPA dataset, the total volume transited at the Fuentes section (blue line, Figure 9.a) is underestimated if compared to the local hydrometer reference (line red), while at the Mallero section (blue line, Figure 9.b) simulated and recorded volumes are in agreement. Also, NSE scores for volumes highlight this fact since Mallero's NSE is ~1 while Fuentes's NSE is about 0.783. Transited volume is the integral of water discharge that CRHyME has better reproduced for the Mallero section (agreement among blue and red line in Figure 9.b and NSE = 0.325) rather than Fuentes's section

600 (disagreement among blue and red line with underestimation of the mean flow during winter periods in Figure 9.b and NSE =  
0.199). Opposite results were obtained considering MERIDA's dataset. There, the Fuentes section has performed well both in  
discharge and volume computation rather than the Mallero section. The volume NSE at Fuentes is now closer to the perfect  
agreement while at Mallero station the transited volume is strongly overestimated. In both cases, NSE scores for discharges  
605 spikes simulated from the ARPA dataset (blue line) are lower compared to the green ones simulated from the MERIDA dataset.  
The CRHyME model performed numerically conservatively in both cases without code instabilities so that these outcomes are  
supposed to be perturbed by the different reconstructions of rainfall fields. From these results can be noticed how the influence  
of rainfall data is determinant in the hydrological assessment. Looking at RMSE scores, the simulation with the ARPA dataset  
was better performed giving lower values of the index, around  $4.7 \text{ m}^3 \text{ s}^{-1}$  and  $45.4 \text{ m}^3 \text{ s}^{-1}$  for the Mallero and Fuentes sections  
610 respectively. This means that discharge uncertainties propagate proportionally increasing the extension of the catchment and  
CRHyME's performances are sensibly higher for small catchments.

Sediment transport results were checked in correspondence with three hydropower reservoirs of Campo Tartano, Valgrosina  
and Cancano (Figure 10.a) considering ARPA dataset simulations. For each reservoir, a literature survey has been conducted  
to estimate the yearly mean sediment accumulation (Ballio et al., 2010; Milanesi et al., 2015; ITCOLD, 2016). The sensitivity  
615 parameter for sediment yield is represented by the slope  $\rightarrow D_{50}$  curve that was adjusted during the calibration period (Figure  
10.b and 10.c). Among others, the set n°6 was retained sufficiently representative of the Valtellina area. In Figure 10.d the  
results obtained from CRHyME simulations are reassumed where the sediment yields evaluated yearly have matched the  
reference data for the three reservoirs investigated. For the Campo Tartano dam, the difference between the simulated and the  
reference is around -11.7%, for the Valgrosina dam is about +2.15% while for the Cancano reservoir is around -11.9%.

620 The capacity of CRHyME to predict the localization of shallow landslides triggered during the events of 1987, 2000 and 2002  
events was investigated through the ROC scores. Figures 11.b, 11.c and 11.d describe the ROC assessment for the shallow  
landslides that occurred across the Valtellina valley during the July 1987, November 2000 and November 2002 events. The  
four shallow landslide instability models included in CRHyME (Iverson, Harp, Milledge, and SLIP) were compared, ranking  
the Harp model as the most accurate one. A realistic combination of friction angle values was considered among the broader  
625 ranges available in the literature (Abbate and Mancusi, 2021a):  $40^\circ$  for gravels,  $35^\circ$  for sand,  $33^\circ$  for silt and  $30^\circ$  for clay  
similar to those proposed by (Crosta and Fratini, 2003). In analogy with root cohesion, the friction angle was spatially  
distributed by considering the soil composition (%coarse, %sand, %silt, %clay) within the superficial layers (Hengl et al.,  
2017). Using the Harp model for the three events, the ROC curves have ranked CRHyME's performance above the "random  
classifier" threshold line. The sensitivity (True Positive Rate) of the model is generally comprised of between 0.2 and 0.6 while  
630 the 1-specificity (False Positive Rate) is around 0.2. The distorted distribution of the shallow landslide inventory related to  
1987 may have influenced the performance predictions, lowering the ROC assessment compared to the events that happened  
in 2000 and 2002. The buffer's choice can influence the redistribution among TP and FP: the performance is lower when large  
buffers are considered, especially for 1000 m and 2000 m radii, while tend to increase with the radius of 250 m and 500 m  
close to the actual extension of shallow landslide recorded.

635



640

**Figure 11:** a) Triggered shallow landslides during the events of July 1987 (yellow points), November 2000 (orange points) and November 2002 (fuchsia points) across the Valtellina area reported by the IFFI inventory. b) Representation of the ROC curves for 1987, 2000 and 2002 events considering the model Harp with different landslide position's buffers. Base layer from © Google Maps 2023.

### 3.3 Emilia case study

For the Emilia case study, CRHyME was tested following a similar schedule for the Valtellina area. Simulations were carried out considering 5 years from 01/09/2011 up to 31/12/2015 where geo-hydrological events of 13/10/2014 and 14/09/2015 have been recorded in the area (Table 6). To raise the model to a realistic initial condition, a spin-up period of 900 days comprised between 01/09/2011 and 28/02/2014 has been carried out. ARPA Emilia meteorological dataset (Rete Monitoraggio ARPA Emilia) was considered for rainfall and temperature variables.

645

Settings for Emilia's catchments	Geo-Hydrological Event Simulated	Starting/Ending Date for the Spin-Up Period		Starting/Ending Date for Validation Period	Rainfall and Temperature Dataset
River Trebbia	September 2015	01/09/2011	28/02/2014	31/12/2015	ARPA Emilia
River Nure	September 2015	01/09/2011	28/02/2014	31/12/2015	ARPA Emilia
River Parma	October 2014	01/09/2011	28/02/2014	31/12/2015	ARPA Emilia

**Table 6:** Simulation settings of the Emilia case study considering the ARPA Emilia rainfall and temperature data.

The hydrology of the Trebbia, Nure and Parma rivers has shown scores similar to the Valtellina area. Looking at NSE in Figure 12.a, we can appreciate that higher scores are assessed for the water volume of Nure (0.978), Parma (0.820) and Trebbia (0.773) rivers. For water discharges, NSE scores are better for Trebbia (0.272) and Parma rivers (0.452) while for Nure River are lower (0.102), also confirmed by the RMSE index (Figure 12.a). Looking at the solid transport quantification, the AdBPo

650

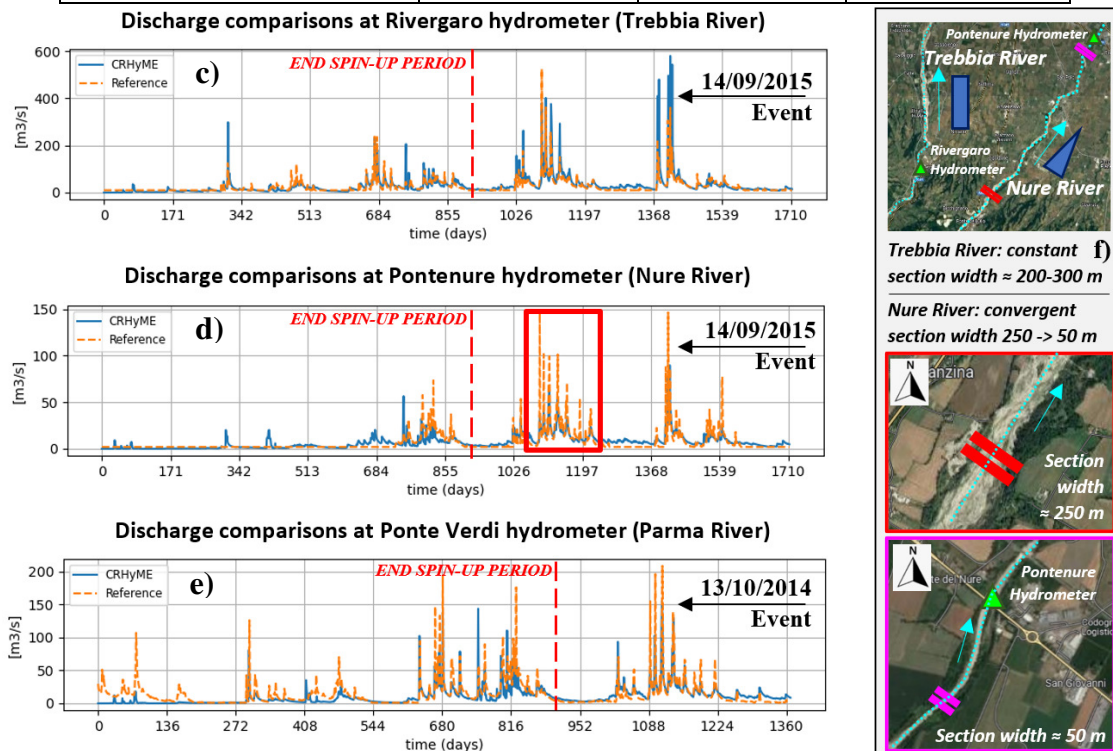
(Autorità di Bacino del fiume Po) reports were taken into consideration as reference data for the comparisons (Autorità di Bacino Distrettuale del Fiume Po, 2022). Keeping the same calibration of the slope  $\rightarrow D_{50}$  curve (set n°6) that was adopted for the Valtellina (no granulometry data were found in the examined catchments), the results obtained after the simulations have shown fairly good accordance with the reference. In the three cases, the order of magnitude of the sediment yield delivered each year at the outlet is similar to AdBPo data especially for Trebbia (+12.6%) and Parma (-24.7%) basins while for Nure we have a slightly larger difference (-35.7%). Perhaps, finer granulometry should have been taken into account for simulating the Parma and Nure rivers, decreasing the  $D_{50}$ . This suggests how the sediment transport dynamics are sensitive to the slope  $\rightarrow D_{50}$  parameterization that strongly depends on the geological and lithological characteristics of the catchment.

a)

Error Analysis of Hydrological Variables	NSE [-]	RMSE [ $\text{m}^3 \text{s}^{-1}$ ]
Discharge Rivergaro (Trebbia River)	0.272	27.915
Volume Rivergaro (Trebbia River)	0.773	-
Discharge Pontenure (Nure River)	0.102	33.468
Volume Pontenure (Nure River)	0.978	-
Discharge Ponte Verdi (Parma River)	0.452	14.898
Discharge Ponte Verdi (Parma River)	0.820	-

b)

Sediment Yield Error Analysis	Trebbia River	Nure River	Parma River
AdbPo Reference	$247.2 \cdot 10^3 \text{ m}^3 \text{ yr}^{-1}$	$69.4 \cdot 10^3 \text{ m}^3 \text{ yr}^{-1}$	$101.1 \cdot 10^3 \text{ m}^3 \text{ yr}^{-1}$
Simulated 2011-2015	$278.3 \cdot 10^3 \text{ m}^3 \text{ yr}^{-1}$	$44.6 \cdot 10^3 \text{ m}^3 \text{ yr}^{-1}$	$76.1 \cdot 10^3 \text{ m}^3 \text{ yr}^{-1}$
% difference	+12.6 %	-35.7 %	-24.7 %



665 **Figure 12: CRHyME model error analysis for hydrological discharge and volume a), sediment yield b) for the Emilia's catchments at c) Rivergaro (Trebbia River), d) Pontenure (Nure River), e) Ponte Verdi (Parma River) hydrometers for the period 2011-2015. The first 900 days of each simulation are considered for model "spin-up" to a realistic initial condition. In the red box d) is highlighted the peak discharge underestimation for the Nure River due to section variation along floodplain f). Base layer from © Google Maps 2023.**

The performance of CRHyME in detecting the triggered debris flow during the events of October 2014 and September 2015 (Figure 13) was assessed again through ROC methodology. A new calibration on the value of the friction angle was carried out since the value provided for the Valtellina was too conservative for stability. This fact could be explained by the Apennines's lithologies which are characterized by higher percentages of clay with respect to the Central Alps that slightly reduce the soil friction resistance (Raj, 1981; Hengl et al., 2017). The highest ROC scores were obtained by slightly decreasing (20%) the slope friction angles and reducing the soil cohesion to the minimum, supposed to be representative of incoherent deposits. In most cases the model has outperformed the random classifier, showing a sensitivity (TPR) comprised between 0.1-0.4 and a higher value of specificity (1-FPR) depending on the chosen buffer extension around the triggering point. In our simulations, debris flow failure has been effectively detected across a small valley impluvium confirming the onsite observations carried out by (Ciccarese et al., 2020; G. et al., 2021).

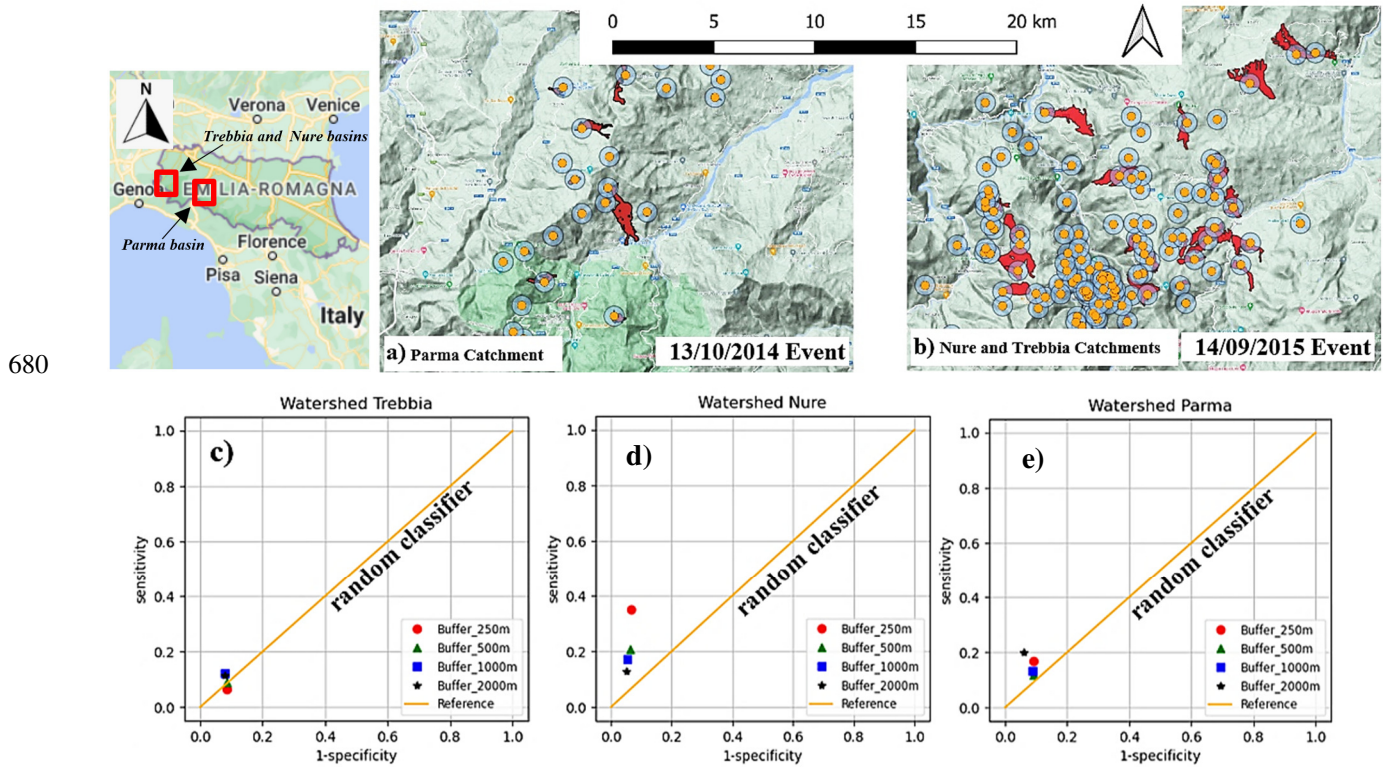


Figure 13: a) Debris flows triggered in the Parma basin during the event of October 2014 and b) debris flows triggered in Trebbia and Nure basins during the event of September 2015. Orange points are the mass wasting starting points reported by (Ciccarese et al., 2020; G. et al., 2021) after the event, blue circles represent a buffer of 500 m around those points and red polygons are historical landslide inventory mapped in the area before the 2014 and 2015 events by the IFFI inventory. Representation of ROC curves for Trebbia c), Nure d) and Parma e) watersheds for the events of October 2014 and September 2015. Base layer from © Google Maps 2023.

## 4 Discussion

### 4.1 CRHyME sensitivity analysis: spatial resolution and sediment diameters

The sensitivity of the CRHyME model in reproducing hydrological cycle has been tested considering four different spatial resolutions within the Caldane catchment (27 km<sup>2</sup>): 90 m, 50 m, 20 m and 5 m. CRHyME results were obtained with sufficient accuracy and faster computation for cell resolution > 10 m. The computational time was observed to be proportional to the number of domain cells: the 90 m, 50 m and 20 m simulations were concluded in one to two minutes while for the 5 m simulation, the time was raised to 5 min. However, increasing spatial resolution doesn't mean always increasing the accuracy (Rocha et al., 2020; Zhang et al., 2016) and with CRHyME the best performance was acquired for spatial resolutions of 50 m and 20 m and not for 5 m. The variation of the DTM resolution can change sensibly the flow direction of the rivers ("ldd.map")

and the basin drainage density, affecting discharge computation. Moreover, according to the literature (López Vicente et al., 2014; Erskine et al., 2006), the routed runoff could be perturbed by “numerical diffusion”, a known problem of the spatially distributed models that is predominant with fine spatial resolution, that depends on the algorithm applied for flow direction computation (Barnes, 2017, 2016). To preserve CRHyME’s solution accuracy and to maintain affordable computational times, we suggest applying the HydroSHED DTM model at 90 m resolution for quite large basins > 500 km<sup>2</sup> while higher resolutions are advisable for smaller basins.

Within the Caldane catchment, the dependence of the sediment transport processes on the soil granulometry was tested. The distribution of  $D_{50}$  that increase as a function of the slope is a reasonable representation of the geomorphological processes that can be encountered in mountain catchments (Brambilla et al., 2020; Ivanov et al., 2020a; Ballio et al., 2010). According to Nino, 2002, among slope and  $D_{50}$  exist a slight correlation, but non-linearities are caused by sediment processes occurring within river granulometry (sorting and armouring). Recently, data-driven approaches were explored in the USA to define a map of the  $D_{50}$  along the river stream (Abeshu et al., 2021). To evaluate the map, these authors have chosen a series of geomorphological predictors of  $D_{50}$  such as slope, elevation etc. verifying results with the available databases at country-based they have retrieved the USA  $D_{50}$  map. Not surprisingly, one of the most important predictors is the basin slope which has the highest correlation coefficient with a  $D_{50}$ . However, the authors stated that other geomorphological factors (river path length and elevation) have a similar correlation with  $D_{50}$ . It seems clear that a unique formulation of the  $D_{50}$  as a function of morphological and hydrodynamical parameters cannot be assessed straightforwardly. Since  $D_{50}$  is required for incipient motion of bed-load sediment transport (Chow et al., 1988), and bearing in mind its complexity in spatial evaluation, slope  $\rightarrow$   $D_{50}$  curves implemented in CRHyME represent a crude but efficacious simplification. Moreover, slope  $\rightarrow$   $D_{50}$  have the advantage of being easily calibrated in the function of on-site data if available.

#### 4.2 CRHyME’s hydrological performances

For the Valtellina case study, CRHyME hydrological performances regarding the water discharge (NSE ~ 0.2-0.3) were not comparable to the ones obtained for the Caldane River (NSE ~ 0.46). A possible explanation resides within the characteristics of the Valtellina catchment, which is bigger (2600 km<sup>2</sup>) than the Caldane basin (27 km<sup>2</sup>). Bigger computation domains mean increased landscape heterogeneity which implies higher uncertainties in the reproduction of infiltration-runoff-groundwater processes (Morbidelli et al., 2018; Mishra et al., 2003; Chow et al., 1988). Comparing volume and discharge scores for the Valtellina area driven by the ARPA dataset, a general tendency to overestimate the peak discharge during rainfall seasons (spring, summer and autumn) can be noticed while an underestimation of the discharges during winter is detected (Figure 9.a). This effect is more significant at the Fuentes hydrometer but is less evident at the Mallero station. After analysing these results, three main error components were disentangled into 1) infiltration, 2) losses, and 3) routing parameterizations. They represent key processes that should be paid attention to during the calibration phase (Morbidelli et al., 2018) since if they are wrong-conditioned may also cause numerical instabilities, losing the balance conservativity of the code. As reported by (Abbate and Mancusi, 2021a), infiltration models strongly regulate runoff generation. Their parameterization depends on land surface coverage and terrain composition which are sometimes affected by high uncertainties since onsite measurements are generally not available and coverage layers have low resolution. For CRHyME, this fact may imply cascade effects on landslide processes causing underestimation of the landslides triggered due to the reduced subsurface pore pressure caused by wrong soil moisture balance predictions. Water recirculation inside the groundwater reservoir generally affects water balance in the long term. In this regard, Alps and Apennines have complex hydrogeology (ISPRA, 2018) which affects the groundwater dynamics that a simple Dupuit model may oversimplify. Unfortunately, the unavailability of local piezometric reference data for calibration has not permitted us to assess model performance for this part. To cope with these uncertainties, several sensitivity and calibration tests (not reported here) were conducted varying groundwater parameterization to achieve the best performances. Another source of error is embedded within the runoff-routing algorithm. The kinematic runoff-routing model



adopted in CRHyME is sufficiently representative of the small lateral catchment rainfall-runoff processes (as for Caldone or  
740 Mallero rivers) but maybe not be suitable for interpreting floodplain flood evolution where dynamic processes are prevalent  
(Chow et al., 1988). Moreover, across the Valtellina catchment, river discharges are regulated by several hydropower plants  
(ITCOLD, 2009, 2016). Dams can smooth and shift floods peaks and perturb seasonal water discharges recorded at the outlet's  
hydrometer lowering the CRHyME performances: in the current version of the model lakes and dams are not considered  
explicitly. Among others, this fact could explain the best score (NSE = 0.325) of the Mallero sub-catchment (less regulated,  
745 only 2 dams) with respect to the Fuentes outlet (NSE = 0.199) for the whole Valtellina catchment (Figure 7).

The hydrological performances of Emilia catchments have scores similar to the Mallero River. The water discharge assessment  
for the tested period shows the best agreement for Trebbia (NSE ~ 0.27) and Parma (NSE ~ 0.45). These basins are less  
regulated by hydropower reservoirs compared to the Valtellina, and, since they are smaller (about 1/3 of the extension), the  
kinematic approach for runoff routing is more representative. Nevertheless, the lower scores for the Nure River are caused by  
750 an underestimation of the peak discharges (Figure 12). Several simulations conducted in the Nure basin have shown a  
systematic bias within the reference data. The latter could be explained by the location of the reference hydrometer, which is  
settled far away across the flood plain where the river is constricted to flow within a narrow section (~10 m) compared to the  
upper catchment (~ 250 m) (Figure 12.f). Looking at Figure 7, the Pontenure (Nure River) hydrometer is located across the  
flood plain ~20 km downstream of the catchment for the Rivergaro (Trebbia River, ~1 km) and the Ponte Verdi (Parma River,  
755 ~10 km) stations. Similarly to the Valtellina case, where a flood lamination is likely to occur, to describe river behaviour  
across a floodplain, the dynamic approach should be preferred instead of kinematic routing. In fact, including section geometry  
as input could increase the simulation accuracy, improving the model's performances in hydrographs and discharge  
reconstruction (Lee and Pin Chun, 2012; Chow et al., 1988).

#### 4.3 CRHyME's geo-hydrological performances

760 Geo-hydrological processes have been physically consistently reproduced by CRHyME. The sediment yields calculated on a  
yearly basis in the Valtellina catchment have matched the available reference data of Campo Tartano, Valgrosina and Cancano  
dams after a calibration of the slope  $\rightarrow D_{50}$  to distribute grain size parameters across the catchment. The good reproduction of  
the annual sediment yield (~ 10% underestimation for Valtellina) has been confirmed also for the Emilia case study where the  
order of magnitude was correctly reproduced compared to the AdBPo reference (~  $\pm 20\%$  depending on the basin).

765 Since the  $D_{50}$  perturbs the threshold that activates the sediment transport (Vetsch et al., 2018), it has revealed the critical  
parameter to be assessed in the CRHyME model. For the Valtellina and Emilia areas, the optimal slope  $\rightarrow D_{50}$  curve was  
rather different compared to the one adopted for the Caldone catchment. From a geological viewpoint, the Caldone catchment  
is in the pre-alps where calcareous rocks are prevalent while metamorphic bedrock is more diffused across the Valtellina  
catchment (ISPRA, 2018). Depending on the state of fracture, metamorphic could be less strength than calcareous and more  
770 prone to be fragmented into small diameters (D'Agostino and Marchi, 2001). Moreover, the maturity of the watershed  
influences the granulometry distribution across the landscape (Pérez-Peña et al., 2009; Strahler, 1952). Large basins such as  
the Valtellina and Emilia catchments are more "mature" than the small Caldone catchment, therefore, a finer granulometry at  
the outlet is expected. This fact seems to justify why a lower slope  $\rightarrow D_{50}$  curve was optimal for these catchments while a  
higher one was more suitable for the Caldone basin.

775 The CRHyME model has identified the localization and the timing of landslide failures during the extreme events that have  
affected the studied catchment. Looking at ROC scores for the Valtellina area, 1987, 2000 and 2002 events were reproduced  
consistently. The best scores were acquired for 2000 and 2002 events also a good quality inventory was available for the  
investigated area. For 1987, as can be appreciated in Figure 11.b, the incompleteness of the available inventory (yellow points)  
has affected the model's final score. However, independently from the specific case, the ROC methodology has highlighted  
780 how much the choice of stability parameters (friction angle and cohesion) has a critical influence on the final results. This fact

has been confirmed also by the sensitivity analysis carried out for debris flow episodes in the Emilia case study during the events of 2014 and 2015. Here, to reach the best ROC scores against the random classifier, the friction angles calibrated for Valtellina have been slightly reduced by about 20% confirming the dependence of this parameter on soil lithology and texture.

#### 4.4 Model limitations

785 The sensibility of the CRHyME model to precipitation mapping, initial conditions settings, DTM scale-dependency and geo-hydrological cycle parametrization have affected result accuracy and performances. Since they represent the current limitations on the widespread applicability of the code a brief discussion is here developed suggesting possible solutions.

790 Correctly assessing the precipitation distribution is mandatory to define a realistic representation of the external forcing that triggers geo-hydrological failures (Abbate et al., 2021b). Especially across mountain regions, the higher local variability of meteorology and the absence of a dense rain gauge network can complicate the reconstruction of a representative rainfall field. This aspect was investigated for the Valtellina case study, where simulations derived by MERIDA (Bonanno et al., 2019) and ARPA (Rete Monitoraggio ARPA Lombardia) datasets were compared. Using MERIDA, we would expect a better performance from CRHyME runs but this didn't happen in all situations. Looking at water volumes transited across the Fuentes hydrometer during the period 2015-2019, the MERIDA dataset has performed better than ARPA stations. On the other hand, 795 looking at the Mallero hydrometer, the MERIDA dataset has scored worse than ARPA stations. What is the possible explanation for this contradictory fact? MERIDA gives a rainfall map that has a spatial resolution of ~ 4 km while the ARPA station data are interpolated geometrically using the Inverse Distance Weight (IDW) techniques (Daly et al., 1997; Chow et al., 1988). A trade-off exists between the ARPA's rain gauge network density and the spatial resolution of MERIDA. In large catchments, MERIDA is more representative since it can cover ungauged areas while in small catchments, lower spatial resolution may be insufficient for describing local rainfall. This is why MERIDA has performed worse than IDW in the Mallero 800 catchment where several ground-based weather stations are uniformly distributed across a limited area of 320 km<sup>2</sup> (Figure 7) Moreover, reanalysis datasets could sometimes smooth the rainfall peaks leading to a wrong interpretation of the net rainfall that occurred over a limited area (Abbate et al., 2021b; Bonanno et al., 2019; Ly et al., 2013). This is another key issue that generally influences the ability performance of the slope stability model implemented in CRHyME to detect landslides 805 triggered by rainfalls. In this regard, a better integration within rainfall sources coming from the ground-based station, reanalysis models, radar maps and satellite data is advisable to reduce possible rainfall uncertainties (Abbate et al., 2021b).

The choice of a realistic initial catchment's moisturizing is another common issue in every deterministic spatially-distributed hydrological model (Uber et al., 2018; Trambly et al., 2010; Chow et al., 1988). Historical measures about the superficial soil moisture, groundwater piezometry and superficial runoff are difficult to gather, especially across small mountain basins where 810 monitoring systems are not provided (Schoener and Stone, 2020; Chiarelli et al., 2023). Moreover, soil moisture is a quantity that can vary abruptly across different terrain types, so it is not common to implement a network that permits the acquisition of distributed information across a catchment (Lazzari et al., 2018). In CRHyME, to overcome these difficulties, a "spin-up period" was introduced within each simulation. This period represents the minimum time required by the model for reaching an automatic adjustment of the initial condition that depending on the extension of the basin, can be comprised within a few 815 months up to some years. In fact, the spin-up simulation permits a re-distribution of the water across the cells of the domain (horizontally) and among each layer of the model (vertically), reducing the "time lag" between rapid (runoff) and slow (groundwater) catchment dynamics. This "time lag" effect was rather evident for the Emilia case study, where a realistic regime condition was reached only after three years, rather slower than for the Adda basin (2 years). This fact could be explained by the different soil compositions and lithology that influence hydrogeological parameters. In the Apennines, the presence of clay 820 decreases the speed of soil recharge (lower permeability) slowing down the groundwater recharge (Ronchetti et al., 2009; Ciccarese et al., 2020; Parenti et al., 2023) compared to the Alps, where coarser terrain granulometry increases soil permeabilities. From a practical viewpoint, running the model up to realistic hydrological conditions is time-consuming. In

CRHyME, PCRaster libraries are already parallelized and can reduce sensibly the computational cost of this operation. Moreover, CRHyME can set a “restart” condition, saving the “main state” outputs of hydrological storage quantities  $\Delta h_{\text{snow}}(t)$ ,  $\Delta h_{\text{soilwater}}(t)$ ,  $\Delta h_{\text{groundwater}}(t)$  and  $\Delta h_{\text{runoff}}(t)$  computed during the spin-up period which could be reused for subsequent running.

For evaluating shallow landslide and debris flow triggering the simple theory of the infinite slope stability model has been implemented. According to the literature (Harp et al., 2006; Iverson, 2000; Takahashi, 2009; Oguz et al., 2022; Milledge et al., 2014), this methodology is rather affordable for cell-based landslide susceptibility models and mapping thanks to its fast coding. However, its strong dependence on DTM resolution represents the main drawback since varying it different results are expected. This fact was not directly experienced with CRHyME since in the Caldane catchment, where spatial scale dependence was tested for the hydrological part, the IFFI inventory was not available for landslides. Legorreta Paulin et al., 2010 and Zheng et al., 2020 have pointed out how the simple infinite slope theory needs to be applied carefully. First of all the inaccuracy of the infinite slope method is related to the fact that each pixel is considered independent from the other settled at the boundary (Iverson, 2000). For very large DTM pixel size, namely  $> 100$  m this may be an acceptable hypothesis since  $100 \times 100 \text{ m}^2$  represents the typical order of magnitude of a rainfall-induced shallow landslide or a debris spatial extension ( $\sim 10^4 \text{ m}^2$ ). For pixels  $\leq 100$  m this is not properly correct since the cell size is lower than the typical dimension: surrounding areas may participate in the landslide collapse due to boundary effects, especially at the top and bottom edges (Figure 5), caused by strength redistribution (Zheng et al., 2020; Milledge et al., 2014). In CRHyME, having a spatial resolution of about  $\sim 70$  m, we have preferred to include the surrounding 8 pixels close to the unstable areas, following a rather conservative choice justified by the physical interpretation of landslide kinematics. On the other hand, varying DTM’s resolution causes a modification of the local slope gradients which are the main drivers of failures: lower resolutions can operate an unphysical smoothing of the surface reducing cliff and scarp that may trigger small landslides. In principle, the best DTM resolution available may lead to the most accurate results but this choice is generally adopted for static landslide susceptibility mapping while may not be suitable for dynamic routines (Legorreta Paulin et al., 2010; Zhang et al., 2016). In CRHyME hydrological balance is computed at each time step and then the slope stability calculation is evaluated recursively: increasing the spatial resolution the computational times rise fast so that a trade-off between model performance and result accuracy should be acquired. Bearing in mind this is a critical issue, improvements are planned in the future version of the code, making the slope stability hazard assessment less scale-dependent and less conservative.

According to Gariano and Guzzetti, 2016a, reconstructing the whole geo-hydrological cycle that drives the erosion and mass wasting processes through numerical models is a challenge. In this regard, CRHyME is not an exception: the EPM is considered for erosion; empirical power-law relationships are implemented for sediment routing; only landslide and debris flow triggering conditions are evaluated by stability models, not including runout evolutions. This subdivision was adopted firstly to simplify the phenomena interactions and secondly to guarantee the fast functioning and stability of the CRHyME code. Following this sequential scheme, geo-hydrological processes are computed after the hydrological assessment, but feedback is not explicitly taken into account. On a long-term timescale, geo-hydrological processes contribute to a landscape modification, e.g. DTM’s height changes. The former is not included by CRHyME since the code has been built with a different purpose with respect to landscape-evolutions models (Campforts et al., 2020; Bovy et al., 2020; Salles, 2019). However, all geo-hydrological hazards also play an important role also on short-term modifying temporarily or permanently the local soil depth (Sklar et al., 2017): landslide and debris flow runout can redistribute the local terrain changing the soil depth (asportation at the crown and accumulation at the toe) and modifying the DTM height. Therefore, finding a “closure” for the superficial geo-hydrological balance is a non-trivial task from a theoretical and numerical viewpoint (D’Odorico and Fagherazzi, 2003). In fact, the CRHyME experience has shown how landslides and debris flow stability assessment cannot be treated deterministically since their triggering strongly depends on stability parameters (the friction angle and the cohesion) which are parameters generally measured on the field or in a laboratory. In CRHyME, following some literature studies (Hengl et al., 2017; Yu et al., 2018;

Chow et al., 1988; Dade and Friend, 1998), the cohesion was spatially distributed in the function of vegetation coverage bearing in mind the roots contribute to stability while the friction angle was correlated with the soil composition. On the other side, friction angle is in function of soil texture, granulometry and consolidation, depending also on complex sediment dynamics and geological processes (de Vente and Poesen, 2005; Merritt et al., 2003; Shobe et al., 2017; Ballio et al., 2010; Kondolf, 870 1997). As a result, the calibration procedure within a sensitivity analysis was necessary case-by-case since these parameters correlate with several geo-morphological predictors. The assessment of the superficial geo-hydrological cycle cannot be evaluated precisely since its monitoring is currently still insufficient on a catchment scale (ISPRA, 2018; Gariano and Guzzetti, 2016). Even though surface mapping and inventory are supposed to increase their accuracy and completeness in the future thanks to remote sensing data (Ciampalini et al., 2016), some doubts remain about possible improvements for other 875 fundamental data required for slope stability and sediment transport spatially distributed models. However, the databases adopted in CRHyME (Hengl et al., 2017; Huscroft et al., 2018; Ross et al., 2018) represent the very first attempt to overcome these issues having already made an important homogenization of the essential data required for geo-hydrological modelling.

## 5 Conclusion

In engineering fields, geo-hydrogeological processes have been conventionally studied separately to make them more tractable 880 for the sake of simplicity. Therefore, hydrological models that assess jointly the erosion, and sediment transport processes and evaluate shallow landslide instabilities are quite rare. In this sense, the CRHyME model was designed as a tool able to show a complete picture of the most significant geo-hydrological processes that may occur at the catchment scale.

CRHyME model was built ex-novo using Python programming language, implementing faster PCRaster libraries that can simulate hydrological processes in a very efficient way. CRHyME includes some of the common features of the classical 885 spatially distributed hydrological model but its focus is on quantitative reconstruction of geo-hydrological hazards. CRHyME is characterized by 6 modules that reproduce hydrological balance over terrain and by a brand-new module deputed to simulate erosion, solid transport, shallow landslide and debris flow triggering at the catchment scale. In the field of geo-hydrological risk assessment, the integration of all those processes in a spatially distributed hydrological model represents a novelty.

Since the aim of our study was to build and facilitate the usage of the model indistinctly in any area of the globe, a deep 890 investigation of the open-source repositories available for initial data has been carried out. The user-defined calibration parameters have been reduced to the minimum. Among them, erosion coefficients, average sediment diameters, cohesion and friction angle have been tuned following the strategies presented above. A sensitivity analysis has been carried out to simplify and accelerate the reconstruction of realistic hydrological initial conditions, adding the possibility to activate the restart option after a spin-up period. Moreover, the DTM's resolution scale dependency was investigated and detected by the results.

CRHyME was intensively tested to make it as general as possible and reproducible in whatever catchments. Our case studies, 895 the Caldane basin, the Valtellina Valley and the Emilia area, were chosen looking at the availability of historical data that is of paramount importance for model validation. The results have shown a fairly good reproduction of the past observations: the model is hydrologically conservative (the volume of water recirculating across the basin is conserved), and numerically stable (thanks to PCRaster libraries); the solid discharge reproduced with downscaled EPM Gavrilovic's method is consistent with 900 the observations, even though there are some uncertainties on  $D_{50}$  parameter; the triggering of shallow landslides and debris flows is comparable in number and spatial localization to the reference inventory. However, CRHyME's performances are rather sensitive to the quality of rainfall field data that should be accurate in spatial and temporal resolution to allow the code to detect correctly possible triggered landslides.

The efforts conducted with the creation of CRHyME go in the direction of a better investigation of geo-hydrological hazards. 905 CRHyME is a multi-hazard model able to address and quantify at catchment scale several geo-hydrological processes that may occur simultaneously, are physically coupled and cannot be interpreted separately. With CRHyME is possible to overcome

the software fragmentation that is currently present in the geo-hydrological field, answering the recent needs required for multi-hazard quantification and multi-risk evaluation not only for back analysis studies but also for now-casting evaluation at the Civil Protection level.

910

## Appendix A

Here, an example of the CRHyME “.INI” file for the simulation setting is reported. Each module has its options where the parameters, variables and other settings required are specified. The “.INI” file essentially reports the simulation time settings (e.g., starting date and ending date), the spatially distributed input data and the meteorological and climatological data series, 915 the settings of each computational module and the name of the output files. The “.INI” file is read by the “deterministic\_runner.py” file that starts the CRHyME model and its internal routines (Figure 2): in “pre-processing.py”, “reporting.py” and “plot.py” modules, variables are respectively defined, saved, and plotted following the formats and standards of the PCRaster libraries (Sutanudjaja et al., 2018; Karssenberg et al., 2010). CRHyME’s results are reported in two formats, as a “.csv” datasheet or a “.netcdf” map (Jacob et al., 2014; Sutanudjaja et al., 2018). The first type is generally used 920 to pick up information of a particular quantity at one location such as in the correspondence of a rain gauge or hydrometric station. The datasheet is organized with a first column containing the time step value while the subsequent columns contain picked information of one or more monitoring points. The “.netcdf” maps are produced to store information about the states and fluxes variables of the model. At each timestep, the quantity at the spatial resolution of the DTM model is saved within the “.netcdf” stack. The required variable to be sampled should be specified in the “.INI” file under the “reporting options”:

925 for “.csv” files a “.map” file containing the location of sample points while for .netcdf the name of the variable required should be specified. Using the GDAL libraries for Python (GDAL/OGR contributors, 2020), the input/output geographical data has been converted to the PCRaster standard format “.map” for raster data (Karssenberg et al., 2010; Sutanudjaja et al., 2018), considering WGS84 datum as a reference system for geographical projection. In the output’s files: the lateral water fluxes  $F_{sub}(t)$ ,  $F_{GW}(t)$  and  $F_{kin-dyn}(t)$  are expressed in  $[m^3s^{-1}]$ ; the vertical water fluxes  $C_l(t)$ ,  $S_{ml}(t)$ ,  $I(t)$ ,  $ETc(t)$ ,  $R(t)$ ,  $L_{per}(t)$ , 930  $Ex(t)$  and  $Ex_{GW}(t)$  are expressed in  $[mm\ day^{-1}]$ ; storage quantities  $\Delta h_{snow}(t)$ ,  $\Delta h_{soilwater}(t)$ ,  $\Delta h_{groundwater}(t)$  and  $\Delta h_{runoff}(t)$  are converted into  $[m^3]$  for volumes simply multiplying the storage height by the cell area extension of the DTM in  $[m^2]$ . Further description of the sub-modules can be found inside the CRHyME’s manual (Abbate and Mancusi, 2021a, b).

### .INI FILE EXAMPLE

935	[globalOptions]	(CRHYME’S GENERAL OPTIONS)
	inputDir = ***\ModelCRHyME\CRHyME_Inputs_Trebbia	(input directory)
	outputDir = ***\ModelCRHyME\CRHyME_Outputs_R	(output directory)
	cloneMap = map\clone.map	(clone map for delimiting domain)
	institution = RSE_Ricerca Sistema Energetico	(institution name)
940	title = CRHyME project	(project title)
	description = by Andrea Abbate and Leonardo Mancusi, resolution = 90 m	(project description)
	resolution = 90	(spatial data resolution)
	startSeries = 1985-12-31	(starting data of series) <sup>1</sup>
	startTime = 1986-01-01	(starting data of simulation) <sup>1</sup>
945	endTime = 2005-12-30	(ending data of simulation) <sup>1</sup>
	timestep = 24	(timestep resolution in hours)
	stampTimestep = 1	(stamp timestep in n° timestep)
	Restart = 1	(activate restart option after spin-up)
	Restart_Snow = \restarts\mod2\Restart_Snow.map	(snow height state for restart)
950	Restart_Surface = \restarts\mod2\Restart_Surface.map	(runoff height state for restart)
	Restart_Soil = \restarts\mod2\Restart_Soil.map	(soil water height state for restart)
	Restart_Ground = \restarts\mod2\Restart_Ground.map	(ground water height state for restart)
	Restart_SoilSed = \restarts\mod2\Restart_SoilSed.map	(sediment height state for restart)

955	[climaOptions] CLIMA_Switch = 1 Rain_NC4 = netcdf\eucoordhi_mod2_pr_day.nc	(CLIMA MODULE OPTIONS) (enable reanalysis-climatic input data) (.netcdf reanalysis-climatic input data)
960	[meteoOptions] input_tab = tab mask = map\mask01.map DTM = map\DTM_clip.map z0 = tss\mod2\Z0_eucoordhi_mod2_tas_day.tss TempRatio = tss\mod2\TCcoef_eucoordhi_mod2_tas_day.tss z0MAX = tss\mod2\Z0_eucoordhi_mod2_tasmax_day.tss TempRatioMAX = tss\mod2\TCcoef_eucoordhi_mod2_tasmax_day.tss z0MIN = tss\mod2\Z0_eucoordhi_mod2_tasmin_day.tss TempRatioMIN = tss\mod2\TCcoef_eucoordhi_mod2_tasmin_day.tss infilRain_file = tss\2011_2016\Rain_TREBBIA_Precipitazione_ALL.tss	(METEO MODULE OPTIONS) (folder containing .tab (txt) datasheet) (0-1 mask map, equal to clone.map) (elevation model dtm.map [m]) (regression temp-elev: intercept) (regression temp-elev: angular coeff.) (intercept for MAX temp.) (angular coeff. for MAX temp.) (intercept for MIN temp.) (angular coeff for MIN temp.) (rain gauges time series .tss (txt)) <sup>2</sup>
970	mayrainstat = map\Rain_Stations_Trebbia.map LAT = 43 ETC_Switch = 1 Aspect = map\Aspect_Filled.map Slope = map\Slope_Filled.map	(rain gauges location .map) <sup>2</sup> (latitude) (evapotranspiration calc. enabled) (aspect file .map [-]) (slope file .map [-])
975	mysoilmap = map\CLC_9Cat.map Kc_FAO = tbl\Kc_FAO.tbl Albedo = tbl\Albedo.tbl	(use of soil.map) (kc coefficient for FAO evapotras.) <sup>3</sup> (albedo coefficient for FAO evapotras.) <sup>3</sup>
980	[interceptionSnowOptions] input_tab = tab LAI_max = tbl\LAI_max.tbl LAI_min = tbl\LAI_min.tbl SNOW_Switch = 1	(SNOW AND INTERCEPTION MODULE OPTIONS) (folder containing .tab (txt) datasheet) (LAI maximum index) <sup>4</sup> (LAI minimum index) <sup>4</sup> (snow calc. enabled)
985	[landSurfaceOptions] input_tab = tab INF_Switch = 2 sand_sup = map\Sand_SUP90C.map silt_sup = map\Silt_SUP90C.map clay_sup = map\Clay_SUP90C.map CoarseFrc_SUP = map\CoarsFrg_SUP90C.map myrivermap = map\PathRiverSM.map Loss_River = tbl\Loss_RIV.tbl Inf_CLC = tbl\Infiltr_CLC.tbl	(LAND SURFACE MODULE OPTIONS) (folder containing .tab (txt) datasheet) (infiltration calc. enabled) <sup>5</sup> (%sand on surface soil at 10cm depth) (%silt on surface soil at 10cm depth) (%clay on surface soil at 10cm depth) (%coarse on surface soil at 10cm depth) (river location .map) <sup>6</sup> (reduction coeff. for river losses) <sup>6</sup> (infiltration coeff. f(soil use))
995	CN_I = map\CN_I.map CN_II = map\CN_II.map CN_III = map\CN_III.map Initial_SM = 0.9 SoilDepth = map\BDRICM_M.map	(SCS-CN method CN I .map) (SCS-CN method CN II .map) (SCS-CN method CN III .map) (initial condition of soil moisture) (soil depth .map [cm])
1000	MaxWatStgTOP = map\TSH1_clip.map  MaxWatStgBTM = map\TSH5_clip.map sand_btm = map\Sand_BTM90C.map silt_btm = map\Silt_BTM90C.map	(%max water storage soil 10cm depth)  (%max water storage soil 1m depth) (%sand on surface soil at 1m depth) (%silt on surface soil at 1m depth)
1005	clay_btm = map\Clay_BTM90C.map CoarseFrc_BTM = map\CoarsFrg_BTM90C.map	(%clay on surface soil at 1m depth) (%coarse on surface soil at 1m depth)

	[groundwaterOptions]	(GROUNDWATER MODULE OPTIONS)
	input_tab = tab	(folder containing .tab (txt) datasheet)
1010	Sr_Falda = 0.8	(initial condition of groundwater table)
	Idro_Map = map\Idrogeology_Emilìa_Trebbia.map	(hydrogeological .map) <sup>7</sup>
	Ks_GLHYMPS_exp = map\GLHYMPS_Emilìa_Trebbia.map	(saturated permeability from GLHYMPS) <sup>7</sup>
	Permeability = tbl\IdrogeologyTabs\Permeability.tbl	(saturated permeability .tbl (txt)) <sup>7</sup>
	Anisotrophy = tbl\IdrogeologyTabs\Anisotrophy.tbl	(anisotropy coefficient .tbl (txt)) <sup>7</sup>
1015	Porosity = tbl\IdrogeologyTabs\Porosity.tbl	(porosity coefficient .tbl (txt)) <sup>7</sup>
	Storativity = tbl\IdrogeologyTabs\Storativity.tbl	(storativity coefficient .tbl (txt)) <sup>7</sup>
	Type_Depth = tbl\IdrogeologyTabs\Type.tbl	(hydrogeological reclassify .tbl(txt)) <sup>7</sup>
	[LandSlidesOptions]	(LANDSLIDE MODULE OPTIONS)
1020	LANDSLIDE_Switch_1 = 2	(Landslide trigger calc. enabled) <sup>8</sup>
	C_Veg = tbl\C_Veg.tbl	(cohesion from vegetation .tbl(txt))
	Surcharge = tbl\Sur_Veg.tbl	(cohesion from vegetation .tbl(txt))
	X_Gavrilovic = tbl\X_Gavrilovic.tbl	(EPM X parameter .tbl(txt)) <sup>9</sup>
	Y_Gavrilovic = tbl\Y_Gavrilovic.tbl	(EPM Y parameter .tbl(txt)) <sup>9</sup>
1025	LithoY_Gavrilovic = map\Idrogeology_Emilìa_Trebbia.map	(EPM Y parameter Lithology .map) <sup>9</sup>
	FI_Gavrilovic = map\Kst_Emilìa_Trebbia.map	(EPM fi parameter .map) <sup>9</sup>
	[routingOptions]	(ROUTING MODULE OPTIONS)
	ROUTING_Switch = 1	(enable calc. routing)
1030	lddMap = map\ldd_clip.map	(ldd.map of flow directions)
	cellAreaMap = map\cellsizeArea.map	(map of cell area extension)
	River_Pit = map\Pit_Point.map	(basin outlet location)
	Strickler = tbl\Ks_Strickler.tbl	(Strickler-Manning coefficient)
	SectionTable = tbl\Dynamic\Sections2.tbl	(section type table .map) <sup>10</sup>
1035	[reportingOptions]	(REPORTING MODULE OPTIONS)
	mysamples_real = map\Idro_Samples_Trebbia.map	(real hydrometers sampling .map)
	mysamples_fake = map\Idro_Samples_F.map	(other hydrometers sampling .map)
	mysamples_solid = map\Solid_Samples.map	(reservoir sampling .map)
1040	outDailyTotNC = CumFails,CumFails_D	(daily counted .netcdf) <sup>11</sup>
	outMonthTotNC = P,Etc	(monthly counted .netcdf)
	outMonthAvgNC = T	(monthly averaged .netcdf)
	outMonthEndNC = CumFails,CumFails_D	(end-monthly counting .netcdf) <sup>11</sup>
	outAnnualTotNC = P,Etc	(annual cumulated .netcdf)
1045	outAnnualAvgNC = T	(monthly averaged .netcdf)
	outAnnuaEndNC = CumFails,CumFails_D	(end-annual cumulated .netcdf) <sup>11</sup>
	formatNetCDF = NETCDF4	(.netcdf specified format)
	zlib = True	(enable .netcdf creation)

ID	Description	Module	Additional References
1	Are specified the starting point of the time series, the starting point of the simulation and the ending point.	[GLOBAL OPTIONS]	-
2	To compute rain gauge simulation, time series in .tss format and a .map of stations are required. Each station has its IDs (1,2,3,...,n) for the corresponding time series with map.	[METEO OPTIONS]	(Karssenberget al., 2010; Sutanudjaja et al., 2018)

3-4	Fao crop coefficient Kc, albedo coefficient and LAI coefficient within .tbl file (a txt table).	[METEO OPTIONS] - [INTERCEPTION SNOW OPTIONS]	(Allan et al., 1998; Nazari et al., 2019)
5	Infiltration model selector: 1) Horton, 2) SCS-SN	[LANDSURFACE OPTIONS]	(Chow et al., 1988)
6	River map derived from PCR flow accumulation and percolation reduction factor below riverbed path.	[LANDSURFACE OPTIONS]	(Chow et al., 1988)
7	Groundwater parameters (.tbl), lithology map and saturated permeability map retrieved from literature and GHYMPS database.	[GROUNDWATER OPTIONS]	(Huscroft et al., 2018; Anderson, 2005; Hayashi, 2020; de Graaf et al., 2015)
8	Landslide model selector: 1) Iverson, 2) Harp, 3) Milledge and 4) SLIP	[LANDSLIDE OPTIONS]	(Iverson, 2000; Montrasio, 2008; Harp et al., 2006; Milledge et al., 2014)
9	EPM parameters from Gavrilovic's method (.tbl and .map)	[LANDSLIDE OPTIONS]	(Milanesi et al., 2015; Panagos et al., 2015)
10	Section table (.tbl) requires for implementation of dynamic routing (experimental)	[ROUTING OPTIONS]	(Karssenbergh et al., 2010; Sutanudjaja et al., 2018)
11	Cumulated shallow landslides and debris flow fails are sampled at yearly/monthly/daily bases	[REPORTING OPTIONS]	-

1050

## Appendix B

Here are reported all the main symbols and their measurement units included in CRHyME (Abbate and Mancusi, 2021a, b).

Main symbols	Description	Units of measurement
<b>A</b>	Hydraulic section area	m <sup>2</sup>
<b><math>\Delta x</math> and <math>\Delta y</math></b>	Cell length and width	m
<b>B</b>	Width of the hydraulic section	m
<b>c</b>	Cohesion of surface soils	kPa
<b>C*</b>	Concentration of debris flows	-
<b>C<sub>i</sub></b>	Canopy Interception	mm day <sup>-1</sup>
<b>CNI CNII CNIII</b>	Curve Numbers SCS-CN for dry-mild-wet conditions	-
<b>D<sub>50</sub></b>	Median diameter of soil grain size	mm
<b>ddf<sub>0</sub></b>	Degree day factor	mm °C <sup>-1</sup> day <sup>-1</sup>
<b>E<sub>s</sub> or W<sub>s</sub></b>	Surface erosion (source parameter for EPM)	mm timestep <sup>-1</sup> or m <sup>3</sup> yr <sup>-1</sup>
<b>Et<sub>0</sub></b>	Potential evapotranspiration	mm timestep <sup>-1</sup>
<b>Et<sub>c</sub></b>	Evapotranspiration	mm timestep <sup>-1</sup>
<b>E<sub>x</sub></b>	Exfiltration	mm timestep <sup>-1</sup>
<b>f<sub>0</sub></b>	Maximum infiltration rate of Horton	mm h <sup>-1</sup>
<b>f<sub>c</sub></b>	Horton's minimum infiltration rate	mm h <sup>-1</sup>
<b>F<sub>gw</sub></b>	Groundwater flow	m <sup>3</sup> s <sup>-1</sup>
<b>F<sub>sub</sub></b>	Subsurface flow	m <sup>3</sup> s <sup>-1</sup>
<b>depth<sub>GW</sub></b>	Groundwater depth	mm or m
<b>depth<sub>soil</sub> or Z</b>	Surface soil depth	mm or m
<b>h<sub>snow</sub></b>	Snow height	mm
<b>h<sub>runoff</sub></b>	Water height at surface	mm
<b>h<sub>soilwater</sub></b>	Water height in surface soil	mm
<b>h<sub>groundwater</sub></b>	Water height in aquifer	mm



<b><math>h_{solid}</math></b>	Sediment height at surface	mm
<b><math>\alpha</math>, slope or <math>i</math></b>	Terrain slope (degrees and dimensionless)	° or %
<b><math>I_a</math></b>	Initial imbibition of the SCS-CN method	mm
<b><math>k</math></b>	Horton decay constant	$h^{-1}$
<b><math>K_c</math></b>	Crop Coefficient	-
<b><math>K_s</math></b>	Hydraulic permeability	$m s^{-1}$
<b><math>K_{Strickler}</math></b>	Strickler roughness coefficient	-
<b>LAI</b>	Leaf Area Index	-
<b><math>L_{per}</math></b>	Percolation	mm timestep <sup>-1</sup>
<b><math>n</math></b>	Porosity	-
<b><math>n_{VG}</math></b>	Van Genuchten n parameter	-
<b><math>P</math></b>	Rainfall	mm timestep <sup>-1</sup>
<b><math>P_n</math></b>	Net Rainfall	mm timestep <sup>-1</sup>
<b><math>F_{kin\_dyn}</math> or <math>Q_l</math></b>	Liquid Discharge	$m^3 s^{-1}$
<b><math>Q_c</math></b>	Critical flow rate of incipient motion for solids	$m^3 s^{-1}$
<b><math>Q_s</math></b>	Solid flow rate	$m^3 s^{-1}$
<b><math>R</math></b>	Runoff	mm timestep <sup>-1</sup>
<b><math>R_{EPM}</math></b>	Routing coefficient for EPM	-
<b><math>S</math></b>	Snow	mm
<b><math>S_{tor}</math></b>	SCS-CN Storativity	mm
<b><math>S_{ml}</math></b>	Snowmelt	mm timestep <sup>-1</sup>
<b><math>S_m</math></b>	Soil Moisture	%
<b><math>T</math></b>	Temperature	°C
<b><math>T_{max}</math> and <math>T_{min}</math></b>	Maximum and minimum temperature	°C
<b><math>T_s</math></b>	Solid Transport	$m^3 s^{-1}$
<b><math>a_x</math> and <math>b_x</math></b>	Parameters of <i>Slope</i> → $D_{50}$ equations	-
<b><math>\alpha_{liquid}</math> e <math>\beta_{liquid}</math></b>	Parameters of the uniform (liquid) flow rate curve	-
<b><math>\alpha_{solid}</math> e <math>\beta_{solid}</math></b>	Parameters of the uniform (solid) flow rate curve	-
<b><math>\phi</math></b>	Friction angle of surface soils	°
<b><math>\theta_s</math> e <math>\theta_r</math></b>	Maximum and minimum surface soil water content	mm or %

### Code and data availability

1055 All the data shown in this paper are freely consultable on Internet websites as reported in the references and within the links we specified through the text. Since the CRHyME code is currently underdeveloped we suggest you contact the main author at this mail [andrea.abbate@rse-web.it](mailto:andrea.abbate@rse-web.it) to receive the most updated and stable copy of the code. For functioning, the CRHyME code requires a Python environment (we suggest Python 3.8 or 3.7 version) and the installation of PCRaster libraries (see the references and links). Further details can be found in (Abbate and Mancusi, 2021a, b).

### Author contributions

1060 AA and LM conceptualized the study. AA carried out the formal analysis and wrote the manuscript with contributions from all co-authors. FA, AF, LL and MP supervised the research, and all the authors reviewed and edited the manuscript.

## Competing interests

The authors declare that they have no conflict of interest.

## Acknowledgements

1065 “This work has been financed by the Research Fund for the Italian Electrical System under the Three-Year Research Plan 2022-2024 (DM MITE n. 337, 15.09.2022), in compliance with the Decree of April 16th, 2018”.

## References

- Abbate, A. and Mancusi, L.: Manuale del modello CRHyME (Climate Rainfall Hydrogeological Modelling Experiment), RSE Report RdS 21012462, Milano, 2021a.
- 1070 Abbate, A. and Mancusi, L.: Strumenti per la mappatura delle minacce idrogeologiche per il sistema energetico e incidenza dei cambiamenti climatici, RSE Report RdS 21010317, Milano, 2021b.
- Abbate, A., Longoni, L., Ivanov, V. I., and Papini, M.: Wildfire impacts on slope stability triggering in mountain areas, *MDPI Geosciences*, 9, 1–15, <https://doi.org/10.3390/geosciences9100417>, 2019.
- 1075 Abbate, A., Papini, M., and Longoni, L.: Analysis of meteorological parameters triggering rainfall-induced landslide: a review of 70 years in Valtellina, *Nat. Hazards Earth Syst. Sci.*, 21, 2041–2058, <https://doi.org/10.5194/nhess-21-2041-2021>, 2021a.
- Abbate, A., Longoni, L., and Papini, M.: Extreme Rainfall over Complex Terrain: An Application of the Linear Model of Orographic Precipitation to a Case Study in the Italian Pre-Alps, 2021, *MDPI Geosciences*, 18, 2021b.
- 1080 Abeshu, G. W., Li, H.-Y., Zhu, Z., Tan, Z., and Leung, L. R.: Median bed-material sediment particle size across rivers in the contiguous U.S., *Earth Syst. Sci. Data Discuss.*, 2021, 1–22, <https://doi.org/10.5194/essd-2021-201>, 2021.
- Allan, R., Pereira, L., and Smith, M.: Crop evapotranspiration-Guidelines for computing crop water requirements-FAO Irrigation and drainage paper 56, 1998.
- 1085 Alvioli, M., Melillo, M., Guzzetti, F., Rossi, M., Palazzi, E., von Hardenberg, J., Brunetti, M. T., and Peruccacci, S.: Implications of climate change on landslide hazard in Central Italy, *Science of The Total Environment*, 630, 1528–1543, <https://doi.org/10.1016/j.scitotenv.2018.02.315>, 2018.
- Ancey, C.: Bedload transport: a walk between randomness and determinism. Part 1. The state of the art, *null*, 58, 1–17, <https://doi.org/10.1080/00221686.2019.1702594>, 2020.
- 1090 Anderson, E. I.: Modeling groundwater–surface water interactions using the Dupuit approximation, *Advances in Water Resources*, 28, 315–327, <https://doi.org/10.1016/j.advwatres.2004.11.007>, 2005.
- Angeli, M. G., Buma, J., Gasparetto, P., and Pasuto, A.: A combined hill slope hydrology/stability model for low-gradient slopes in the Italian Dolomites, *Engineering Geology*, 49, 1–13, [https://doi.org/10.1016/S0013-7952\(97\)00033-1](https://doi.org/10.1016/S0013-7952(97)00033-1), 1998.
- Rete Monitoraggio ARPA Emilia: <https://www.arpae.it/it/temi-ambientali/meteo>.
- 1095 Rete Monitoraggio ARPA Lombardia: [www.arpalombardia.it/stiti/arpalombardia/meteo](http://www.arpalombardia.it/stiti/arpalombardia/meteo).
- Autorità di Bacino Distrettuale del Fiume Po: Linee Generali di Assetto Idrogeologico e Quadro degli Interventi, 2022.
- Ballio, F., Brambilla, D., Giorgetti, E., Longoni, L., Papini, M., and Radice, A.: Evaluation of sediment yield from valley slopes: A case study, 149 pp., <https://doi.org/10.2495/DEB100131>, 2010.

- 1100 Bancheri, M., Rigon, R., and Manfreda, S.: The GEOframe-NewAge Modelling System Applied in a Data Scarce Environment, *Water*, 12, <https://doi.org/10.3390/w12010086>, 2020.
- Barnes, R.: Parallel Priority-Flood depression filling for trillion cell digital elevation models on desktops or clusters, *Computers & Geosciences*, 96, 56–68, <https://doi.org/10.1016/j.cageo.2016.07.001>, 2016.
- Barnes, R.: Parallel non-divergent flow accumulation for trillion cell digital elevation models on desktops or clusters, *Environmental Modelling & Software*, 92, 202–212, <https://doi.org/10.1016/j.envsoft.2017.02.022>, 2017.
- 1105 Bemporad, G. A., Alterach, J., Amighetti, F. F., Peviani, M., and Saccardo, I.: A distributed approach for sediment yield evaluation in Alpine regions, *Journal of Hydrology*, 197, 370–392, [https://doi.org/10.1016/0022-1694\(95\)02978-8](https://doi.org/10.1016/0022-1694(95)02978-8), 1997.
- Berg, J. H.: Prediction of Alluvial Channel Pattern of Perennial Rivers, *Geomorphology*, 12, 259–279, 1110 [https://doi.org/10.1016/0169-555X\(95\)00014-V](https://doi.org/10.1016/0169-555X(95)00014-V), 1995.
- Bonanno, R., Lacavalla, M., and Sperati, S.: A new high-resolution Meteorological Reanalysis Italian Dataset: MERIDA, *Quarterly Journal of the Royal Meteorological Society*, 145, 1756–1779, <https://doi.org/10.1002/qj.3530>, 2019.
- Bordoni, M., Meisina, C., Valentino, R., Lu, N., Bittelli, M., and Chersich, S.: Hydrological factors affecting rainfall-induced shallow landslides: From the field monitoring to a simplified slope stability analysis, *Engineering Geology*, 193, <https://doi.org/10.1016/j.enggeo.2015.04.006>, 2015.
- 1115 Bovolo, C. I. and Bathurst, J. C.: Modelling catchment-scale shallow landslide occurrence and sediment yield as a function of rainfall return period, *Hydrological Processes*, 26, 579–596, <https://doi.org/10.1002/hyp.8158>, 2012.
- Bovy, B., Braun, J., Cordonnier, G., Lange, R., and Yuan, X.: The FastScape software stack: Reusable tools for landscape evolution modelling, in: EGU General Assembly Conference Abstracts, 9474, 2020.
- 1120 Bozzolan, E., Holcombe, E., Pianosi, F., and Wagener, T.: Including informal housing in slope stability analysis – an application to a data-scarce location in the humid tropics, *Natural Hazards and Earth System Sciences*, 20, 3161–3177, <https://doi.org/10.5194/nhess-20-3161-2020>, 2020.
- Brambilla, D., Papini, M., Ivanov, V. I., Bonaventura, L., Abbate, A., and Longoni, L.: Sediment Yield in Mountain Basins, Analysis, and Management: The SMART-SED Project, in: *Applied Geology: Approaches to Future Resource Management*, edited by: De Maio, M. and Tiwari, A. K., Springer International Publishing, Cham, 43–59, [https://doi.org/10.1007/978-3-030-43953-8\\_3](https://doi.org/10.1007/978-3-030-43953-8_3), 2020.
- Bresciani, E., Davy, P., and de Dreuzy, J.-R.: Is the Dupuit assumption suitable for predicting the groundwater seepage area in hillslopes?, *Water Resources Research*, 50, 2394–2406, <https://doi.org/10.1002/2013WR014284>, 1130 2014.
- Campforts, B., Shobe, C., Steer, P., Vanmaercke, M., LAGUE, D., and Braun, J.: HyLands 1.0: a Hybrid Landscape evolution model to simulate the impact of landslides and landslide-derived sediment on landscape evolution, *Geoscientific Model Development*, 13, 3863–3886, 2020.
- Cazorzi, F. and Dalla Fontana, G.: Snowmelt modelling by combining air temperature and a distributed radiation index, *Journal of Hydrology*, 181, 169–187, [https://doi.org/10.1016/0022-1694\(95\)02913-3](https://doi.org/10.1016/0022-1694(95)02913-3), 1996.
- 1135 Ceriani, M., Lauzi, S., and Padovan, M.: Rainfall thresholds triggering debris-flow in the alpine area of Lombardia Region, central Alps – Italy, in: *In Proceedings of the Man and Mountain’94, First International Congress for the Protection and Development of Mountain Environmen*, Ponte di Legno (BS), Italy, 1994.
- Chen, L. and Young, M. H.: Green-Ampt infiltration model for sloping surfaces, *Water Resources Research*, 42, 1140 <https://doi.org/10.1029/2005WR004468>, 2006.

- Chiarelli, D. D., Galizzi, M., Bocchiola, D., Rosso, R., and Rulli, M. C.: Modeling snowmelt influence on shallow landslides in Tartano valley, Italian Alps, *Science of The Total Environment*, 856, 158772, <https://doi.org/10.1016/j.scitotenv.2022.158772>, 2023.
- Chow, V. T., Maidment, D. R., and Mays, L. W.: *Applied hydrology*, McGraw-Hill, New York, 1988.
- 1145 Ciampalini, A., Raspini, F., Lagomarsino, D., Catani, F., and Casagli, N.: Landslide susceptibility map refinement using PSInSAR data, *Remote Sensing of Environment*, 184, 302–315, <https://doi.org/10.1016/j.rse.2016.07.018>, 2016.
- Ciccarese, G., Mulas, M., Alberoni, P. P., Truffelli, G., and Corsini, A.: Debris flows rainfall thresholds in the Apennines of Emilia-Romagna (Italy) derived by the analysis of recent severe rainstorms events and regional meteorological data, *Geomorphology*, 358, 107097, <https://doi.org/10.1016/j.geomorph.2020.107097>, 2020.
- 1150 Cislighi, A., Chiaradia, E. A., and Bischetti, G. B.: Including root reinforcement variability in a probabilistic 3D stability model, *Earth Surface Processes and Landforms*, 42, 1789–1806, <https://doi.org/10.1002/esp.4127>, 2017.
- CNR and IRPI: *Rapporto Periodico sul Rischio posto alla Popolazione italiana da Frane e Inondazioni*, Anno 2020, 19 pp., <https://doi.org/10.30437/report2020>, 2021.
- 1155 Collischonn, W., Fleischmann, A., Paiva, R. C. D., and Mejia, A.: Hydraulic Causes for Basin Hydrograph Skewness, *Water Resources Research*, 53, 10603–10618, <https://doi.org/10.1002/2017WR021543>, 2017.
- Crosta, G. B. and Frattini, P.: Distributed modelling of shallow landslides triggered by intense rainfall, *Natural Hazards and Earth System Sciences*, 3, 81–93, <https://doi.org/10.5194/nhess-3-81-2003>, 2003.
- Crosta, G. B., Imposimato, S., and Roddeman, D. G.: Numerical modelling of large landslides stability and runout, 1160 *Nat. Hazards Earth Syst. Sci.*, 3, 523–538, <https://doi.org/10.5194/nhess-3-523-2003>, 2003.
- Dade, W. B. and Friend, P. F.: Grain-Size, Sediment-Transport Regime, and Channel Slope in Alluvial Rivers, *The Journal of Geology*, 106, 661–676, <https://doi.org/10.1086/516052>, 1998.
- D’Agostino, V. and Marchi, L.: Debris flow magnitude in the Eastern Italian Alps: Data collection and analysis, *Physics and Chemistry of the Earth, Part C: Solar, Terrestrial & Planetary Science*, 26, 657–663, 1165 [https://doi.org/10.1016/S1464-1917\(01\)00064-2](https://doi.org/10.1016/S1464-1917(01)00064-2), 2001.
- Daly, C., Taylor, G., and Gibson, W.: *The PRISM Approach to Mapping Precipitation and Temperature*, 1997.
- Daly, C., Slater, M. E., Roberti, J. A., Laseter, S. H., and Swift Jr, L. W.: High-resolution precipitation mapping in a mountainous watershed: ground truth for evaluating uncertainty in a national precipitation dataset, *International Journal of Climatology*, 37, 124–137, <https://doi.org/10.1002/joc.4986>, 2017.
- 1170 Davolio, S., Della Fera, S., Laviola, S., Miglietta, M. M., and Levizzani, V.: Heavy precipitation over Italy from the Mediterranean storm “Vaia” in October 2018: Assessing the role of an atmospheric river, *Monthly Weather Review*, 148, 3571–3588, 2020.
- Davy, P. and Lague, D.: Fluvial erosion/transport equation of landscape evolution models revisited, *Journal of Geophysical Research: Earth Surface*, 114, <https://doi.org/10.1029/2008JF001146>, 2009.
- 1175 De Vita, P., Fusco, F., Tufano, R., and Cusano, D.: Seasonal and Event-Based Hydrological and Slope Stability Modeling of Pyroclastic Fall Deposits Covering Slopes in Campania (Southern Italy), *Water*, 10, 1140, <https://doi.org/10.3390/w10091140>, 2018.
- Devia, G. K., Ganasri, B. P., and Dwarakish, G. S.: A Review on Hydrological Models, *Aquatic Procedia*, 4, 1001–1007, <https://doi.org/10.1016/j.aqpro.2015.02.126>, 2015.
- 1180 D’Odorico, P. and Fagherazzi, S.: A probabilistic model of rainfall-triggered shallow landslides in hollows: A long-term analysis, *Water Resources Research*, 39, <https://doi.org/10.1029/2002WR001595>, 2003.

- Erskine, R. H., Green, T. R., Ramirez, J. A., and MacDonald, L. H.: Comparison of grid-based algorithms for computing upslope contributing area, *Water Resources Research*, 42, <https://doi.org/10.1029/2005WR004648>, 2006.
- 1185 Fan, Y., Miguez-Macho, G., Weaver, C. P., Walko, R., and Robock, A.: Incorporating water table dynamics in climate modeling: 1. Water table observations and equilibrium water table simulations, *Journal of Geophysical Research: Atmospheres*, 112, <https://doi.org/10.1029/2006JD008111>, 2007.
- Fawcett, T.: An introduction to ROC analysis, *Pattern Recognition Letters*, 27, 861–874, <https://doi.org/10.1016/j.patrec.2005.10.010>, 2006.
- 1190 Formetta, G., Capparelli, G., and Versace, P.: Evaluating performance of simplified physically based models for shallow landslide susceptibility, *Hydrology and Earth System Sciences*, 20, 4585–4603, <https://doi.org/10.5194/hess-20-4585-2016>, 2016.
- G., C., M., M., and A., C.: Combining spatial modelling and regionalization of rainfall thresholds for debris flows hazard mapping in the Emilia-Romagna Apennines (Italy), *Landslides*, 18, 3513–3529, 1195 <https://doi.org/10.1007/s10346-021-01739-w>, 2021.
- Gao, L., Zhang, L. M., and Cheung, R. W. M.: Relationships between natural terrain landslide magnitudes and triggering rainfall based on a large landslide inventory in Hong Kong, *Landslides*, 15, 727–740, <https://doi.org/10.1007/s10346-017-0904-x>, 2018.
- Gariano, S. L. and Guzzetti, F.: Landslides in a changing climate, *Earth-Science Reviews*, 162, 227–252, 1200 <https://doi.org/10.1016/j.earscirev.2016.08.011>, 2016.
- GDAL/OGR contributors: GDAL/OGR Geospatial Data Abstraction software Library, Open Source Geospatial Foundation, 2020.
- Girard, M.-C., Girard, C., Dominique, C., Gilliot, J.-M., Loubersac, L., Meyer-Roux, J., Monget, J.-M., Seguin, B., and Rao, N.: Corine Land Cover, 331–344, <https://doi.org/10.1201/9780203741917-19>, 2018.
- 1205 Gleick, P. H.: Climate change, hydrology, and water resources, *Reviews of Geophysics*, 27, 329–344, <https://doi.org/10.1029/RG027i003p00329>, 1989.
- Globevnik, L., Holjevč, D., Petkovaek, G., and Rubinč, J.: 145. Applicability of the Gavrilovic Method in Erosion Calculation Using Spatial Data Manipulation Techniques, *Tunnelling and Underground Space Technology*, 14, 2003.
- 1210 Govers, G.: Empirical relationships for the transport capacity of overland flow., 1989.
- Govers, G., Wallings, D. E., Yair, A., and Berkowicz, S.: Empirical relationships for the transport capacity of overland flow, *International Association of Hydrological Sciences*, 189, 1990.
- de Graaf, I. E. M., Sutanudjaja, E. H., van Beek, L. P. H., and Bierkens, M. F. P.: A high-resolution global-scale groundwater model, *Hydrol. Earth Syst. Sci.*, 19, 823–837, <https://doi.org/10.5194/hess-19-823-2015>, 2015.
- 1215 Groenendyk, D. G., Ferré, T. P. A., Thorp, K. R., and Rice, A. K.: Hydrologic-Process-Based Soil Texture Classifications for Improved Visualization of Landscape Function., *PLoS One*, 10, e0131299, <https://doi.org/10.1371/journal.pone.0131299>, 2015.
- 1220 Guadagno, M., IRPI CNR, P., Guzzetti, I., Reichenbach, I., and Tonelli, I.: SICI-Sistema Informativo Catastrofi Idrogeologiche-Istituto di Ricerca per la Protezione Idrogeologica (IRPI) del Consiglio Nazionale delle Ricerche e Gruppo Nazionale per la Difesa dalle Catastrofi Idrogeologiche (GNDCI) del Consiglio Nazionale delle Ricerche, 2003.
- Gudiyangada Nachappa, T., Tavakkoli Piralilou, S., Ghorbanzadeh, O., Shahabi, H., and Blaschke, T.: Landslide Susceptibility Mapping for Austria Using Geons and Optimization with the Dempster-Shafer Theory, *Applied Sciences*, 9, <https://doi.org/10.3390/app9245393>, 2019.

- 1225 Guzzetti, F. and Tonelli, G.: Information system on hydrological and geomorphological catastrophes in Italy (SICI): a tool for managing landslide and flood hazards, *Natural Hazards and Earth System Sciences*, 4, 213–232, 2004.
- Guzzetti, F., Reichenbach, P., Cardinali, M., Galli, M., and Ardizzone, F.: Probabilistic landslide hazard assessment at the basin scale, *Geomorphology*, 72, 272–299, <https://doi.org/10.1016/j.geomorph.2005.06.002>, 2005.
- 1230 Guzzetti, F., Peruccacci, S., Rossi, M., and Stark, C. P.: Rainfall thresholds for the initiation of landslides in central and southern Europe, *Meteorology and Atmospheric Physics*, 98, 239–267, <https://doi.org/10.1007/s00703-007-0262-7>, 2007.
- Harp, E. L., Michael, J. A., and Laprade, W. T.: Shallow-landslide hazard map of Seattle, Washington, Reston, VA, <https://doi.org/10.3133/ofr20061139>, 2006.
- 1235 Hayashi, M.: Alpine Hydrogeology: The Critical Role of Groundwater in Sourcing the Headwaters of the World, *Groundwater*, 58, 498–510, <https://doi.org/10.1111/gwat.12965>, 2020.
- Hengl, T., Mendes de Jesus, J., Heuvelink, G. B. M., Ruiperez Gonzalez, M., Kilibarda, M., Blagotić, A., Shangguan, W., Wright, M. N., Geng, X., Bauer-Marschallinger, B., Guevara, M. A., Vargas, R., MacMillan, R. A., Batjes, N. H., Leenaars, J. G. B., Ribeiro, E., Wheeler, I., Mantel, S., and Kempen, B.: SoilGrids250m: Global gridded soil information based on machine learning, *PLOS ONE*, 12, e0169748, <https://doi.org/10.1371/journal.pone.0169748>, 2017.
- 1240 Herrera, M.: Landslide Detection using Random Forest Classifier, <https://doi.org/10.13140/RG.2.2.31365.91369>, 2019.
- Huscroft, J., Gleeson, T., Hartmann, J., and Börker, J.: Compiling and Mapping Global Permeability of the Unconsolidated and Consolidated Earth: GLobal HYdrogeology MaPS 2.0 (GLHYMPS 2.0), *Geophysical Research Letters*, 45, <https://doi.org/10.1002/2017GL075860>, 2018.
- 1245 Iida, T.: A stochastic hydro-geomorphological model for shallow landsliding due to rainstorm, *CATENA*, 34, 293–313, [https://doi.org/10.1016/S0341-8162\(98\)00093-9](https://doi.org/10.1016/S0341-8162(98)00093-9), 1999.
- ISPRA: Dissesto idrogeologico in Italia: pericolosità e indicatori di rischio, ISPRA, Ispra, 2018.
- 1250 ITCOLD: La gestione dell'interrimento dei serbatoi artificiali italiani, Comitato Nazionale Italiano delle Grandi Dighe, 2009.
- ITCOLD: La gestione dell'interrimento dei serbatoi artificiali italiani situazione attuale e prospettive, Comitato Nazionale Italiano delle Grandi Dighe, 2016.
- 1255 Ivanov, V., Radice, A., Papini, M., and Longoni, L.: Event-scale pebble mobility observed by RFID tracking in a pre-Alpine stream: a field laboratory, *Earth Surface Processes and Landforms*, 45, 535–547, <https://doi.org/10.1002/esp.4752>, 2020a.
- Ivanov, V., Arosio, D., Tresoldi, G., Hojat, A., Zanzi, L., Papini, M., and Longoni, L.: Investigation on the Role of Water for the Stability of Shallow Landslides-Insights from Experimental Tests, *Water*, 12(4), 2020b.
- 1260 Iverson, R., Reid, M., and Lahusen, R.: Debris-flow mobilization from landslides. *Annu Rev Earth Planet Sci*, 25, 85–138, <https://doi.org/10.1146/annurev.earth.25.1.85>, 1997.
- Iverson, R. M.: Landslide triggering by rain infiltration, *Water Resources Research*, 36, 1897–1910, <https://doi.org/10.1029/2000WR900090>, 2000.
- Jackson, C. R., Bitew, M., and Du, E.: When interflow also percolates: downslope travel distances and hillslope process zones, *Hydrological Processes*, 28, 3195–3200, <https://doi.org/10.1002/hyp.10158>, 2014.
- 1265 Jacob, D., Petersen, J., Eggert, B., Alias, A., Christensen, O. B., Bouwer, L. M., Braun, A., Colette, A., Déqué, M., Georgievski, G., Georgopoulou, E., Gobiet, A., Menut, L., Nikulin, G., Haensler, A., Hempelmann, N., Jones, C.,

- Keuler, K., Kovats, S., Kröner, N., Kotlarski, S., Kriegsmann, A., Martin, E., van Meijgaard, E., Moseley, C., Pfeifer, S., Preuschmann, S., Radermacher, C., Radtke, K., Rechid, D., Rounsevell, M., Samuelsson, P., Somot, S., Soussana, J.-F., Teichmann, C., Valentini, R., Vautard, R., Weber, B., and Yiou, P.: EURO-CORDEX: new high-resolution climate change projections for European impact research, *Regional Environmental Change*, 14, 563–578, <https://doi.org/10.1007/s10113-013-0499-2>, 2014.
- Jakob, M. and Hungr, O.: *Debris-Flow Hazards and Related Phenomena*, 2005.
- Jakob, M. and Jordan, P.: Design flood estimates in mountain streams – the need for a geomorphic approach, *Can. J. Civ. Eng.*, 28, 425–439, <https://doi.org/10.1139/l01-010>, 2001.
- 1275 Jie, T., Zhang, B., He, C., and Yang, L.: Variability In Soil Hydraulic Conductivity And Soil Hydrological Response Under Different Land Covers In The Mountainous Area Of The Heihe River Watershed, Northwest China, *Land Degradation & Development*, 28, <https://doi.org/10.1002/ldr.2665>, 2016.
- Kadavi, P., Lee, C.-W., and Lee, S.: Application of Ensemble-Based Machine Learning Models to Landslide Susceptibility Mapping, *Remote Sensing*, 10, 1252, <https://doi.org/10.3390/rs10081252>, 2018.
- 1280 Karssenber, D., Schmitz, O., Salamon, P., de Jong, K., and Bierkens, M. F. P.: A software framework for construction of process-based stochastic spatio-temporal models and data assimilation, *Environmental Modelling & Software*, 25, 489–502, <https://doi.org/10.1016/j.envsoft.2009.10.004>, 2010.
- Kim, K.-S., Kim, M.-I., Lee, M.-S., and Hwang, E.-S.: Regression Equations for Estimating Landslide-Triggering Factors Using Soil Characteristics, *Applied Sciences*, 10, <https://doi.org/10.3390/app10103560>, 2020.
- 1285 Klaus, J. and Jackson, C. R.: Interflow Is Not Binary: A Continuous Shallow Perched Layer Does Not Imply Continuous Connectivity, *Water Resources Research*, 54, 5921–5932, <https://doi.org/10.1029/2018WR022920>, 2018.
- Kobierska, F., Jonas, T., Kirchner, J. W., and Bernasconi, S. M.: Linking baseflow separation and groundwater storage dynamics in an alpine basin (Dammagletscher, Switzerland), *Hydrol. Earth Syst. Sci.*, 19, 3681–3693, <https://doi.org/10.5194/hess-19-3681-2015>, 2015.
- 1290 Kondolf, george 'mathias: Hungry Water: Effects of Dams and Gravel Mining on River Channels, *Environmental Management*, 21, 533–551, <https://doi.org/10.1007/s002679900048>, 1997.
- Lamb, M. P. and Venditti, J. G.: The grain size gap and abrupt gravel-sand transitions in rivers due to suspension fallout, *Geophysical Research Letters*, 43, 3777–3785, <https://doi.org/10.1002/2016GL068713>, 2016.
- 1295 Langland, M. J.: Bathymetry and Sediment-Storage Capacity Change in Three Reservoirs on the Lower Susquehanna River, 1996-2008, <https://doi.org/10.3133/sir20095110>, 2009.
- Lazzari, M., Piccarreta, M., and Manfreda, S.: The role of antecedent soil moisture conditions on rainfall-triggered shallow landslides, *Natural Hazards and Earth System Sciences Discussions*, 2018, 1–11, <https://doi.org/10.5194/nhess-2018-371>, 2018.
- 1300 Lee, K. and Pin Chun, H.: Evaluating the adequateness of kinematic-wave routing for flood forecasting in midstream channel reaches of Taiwan, *Journal of Hydroinformatics*, 14, 1075, <https://doi.org/10.2166/hydro.2012.093>, 2012.
- Legorreta Paulin, G., Bursik, M., Lugo-Hubp, J., and Zamorano Orozco, J. J.: Effect of pixel size on cartographic representation of shallow and deep-seated landslide, and its collateral effects on the forecasting of landslides by SINMAP and Multiple Logistic Regression landslide models, *Physics and Chemistry of the Earth, Parts A/B/C*, 35, 137–148, <https://doi.org/10.1016/j.pce.2010.04.008>, 2010.
- Lehner, B., Verdin, K., and Jarvis, A.: New Global Hydrography Derived From Spaceborne Elevation Data, *Eos, Transactions American Geophysical Union*, 89, 93–94, <https://doi.org/10.1029/2008EO100001>, 2008.

- Li, X., Xiao, Q., Niu, J., Dymond, S., McPherson, E. G., van Doorn, N., Yu, X., Xie, B., Zhang, K., and Li, J.:  
1310 Rainfall interception by tree crown and leaf litter: An interactive process, *Hydrological Processes*, 31, 3533–3542,  
<https://doi.org/10.1002/hyp.11275>, 2017.
- Longoni, L., Ivanov, V. I., Brambilla, D., Radice, A., and Papini, M.: Analysis of the temporal and spatial scales  
of soil erosion and transport in a Mountain Basin, *Italian Journal of Engineering Geology and Environment*, 16,  
17–30, <https://doi.org/10.4408/IJEGE.2016-02.O-02>, 2016.
- 1315 López Vicente, M., Pérez-Bielsa, C., López-Montero, T., Lambán, L. J., and Navas, A.: Runoff simulation with  
eight different flow accumulation algorithms: Recommendations using a spatially distributed and open-source  
model, *Environ. Model. Softw.*, 62, 11–21, 2014.
- Luino, F.: Sequence of instability processes triggered by heavy rainfall in the Northern Italy, *Geomorphology*, 66,  
13–39, <https://doi.org/10.1016/j.geomorph.2004.09.010>, 2005.
- 1320 Ly, S., Charles, C., and Degre, A.: Different methods for spatial interpolation of rainfall data for operational  
hydrology and hydrological modeling at watershed scale. A review, *Biotechnology, Agronomy and Society and  
Environment*, 17, 392–406, 2013.
- Marnezy, A.: Alpine dams. From hydroelectric power to artificial snow, *Revue de géographie alpine*, 96, 2008.
- Meisina, C., Zizioli, D., and Zucca, F.: Methods for Shallow Landslides Susceptibility Mapping: An Example in  
1325 Oltrepo Pavese, 1, 451–457, <https://doi.org/10.1007/978-3-642-31325-7-58>, 2013.
- Merritt, W. S., Letcher, R. A., and Jakeman, A. J.: A review of erosion and sediment transport models,  
*Environmental Modelling & Software*, 18, 761–799, [https://doi.org/10.1016/S1364-8152\(03\)00078-1](https://doi.org/10.1016/S1364-8152(03)00078-1), 2003.
- Michel, G. P., Kobiyama, M., and Goerl, R. F.: Comparative analysis of SHALSTAB and SINMAP for landslide  
susceptibility mapping in the Cunha River basin, southern Brazil, *Journal of Soils and Sediments*, 14, 1266–1277,  
1330 <https://doi.org/10.1007/s11368-014-0886-4>, 2014.
- Milanesi, L., Pilotti, M., Clerici, A., and Gavrilovic, Z.: Application of an improved version of the Erosion Potential  
Method in Alpine areas, *Italian Journal of Engineering Geology and Environment*,  
<https://doi.org/10.4408/IJEGE.2015-01.O-02>, 2015.
- Milledge, D. G., Bellugi, D., McKean, J. A., Densmore, A. L., and Dietrich, W. E.: A multidimensional stability  
1335 model for predicting shallow landslide size and shape across landscapes, *Journal of Geophysical Research: Earth  
Surface*, 119, 2481–2504, <https://doi.org/10.1002/2014JF003135>, 2014.
- Mishra, S. K., Tyagi, J. V., and Singh, V. P.: Comparison of infiltration models, *Hydrological Processes*, 17, 2629–  
2652, <https://doi.org/10.1002/hyp.1257>, 2003.
- Moges, E., Demissie, Y., Larsen, L., and Yassin, F.: Review: Sources of Hydrological Model Uncertainties and  
1340 Advances in Their Analysis, *Water*, 13, <https://doi.org/10.3390/w13010028>, 2021.
- Montrasio, L.: Stability of soil-slip, Wit Press, *Risk Analysis II*, 45, 357–366, <https://doi.org/10.2495/RISK000331>,  
2008.
- Montrasio, L. and Valentino, R.: Modelling Rainfall-induced Shallow Landslides at Different Scales Using SLIP -  
Part II, *Procedia Engineering*, 158, 482–486, <https://doi.org/10.1016/j.proeng.2016.08.476>, 2016.
- 1345 Morbidelli, R., Corradini, C., Saltalippi, C., Flammini, A., Dari, J., and Govindaraju, R. S.: Rainfall Infiltration  
Modeling: A Review, *Water*, 10, <https://doi.org/10.3390/w10121873>, 2018.
- Morgan, R. P. C. and Nearing, M. A.: *Handbook of erosion modelling.*, 2011.
- Munich Re: Natural disasters caused overall losses of US \$ 210bn Relevant natural catastrophe loss events  
worldwide 2020, 1, 2021.



- 1350 Nazari, M., Sadeghi, S. M. M., Van Stan, J., and Chaichi, M.: Rainfall interception and redistribution by maize farmland in central Iran, *Journal of Hydrology: Regional Studies*, 27, 100656, <https://doi.org/10.1016/j.ejrh.2019.100656>, 2019.
- Nino, Y.: Simple Model for Downstream Variation of Median Sediment Size in Chilean Rivers, *Journal of Hydraulic Engineering*, 128, 934–941, 2002.
- 1355 Oguz, E. A., Depina, I., and Thakur, V.: Effects of soil heterogeneity on susceptibility of shallow landslides, *Landslides*, 19, 67–83, <https://doi.org/10.1007/s10346-021-01738-x>, 2022.
- Pacina, J., Lendáková, Z., Štojdl, J., Matys Grygar, T., and Dolejš, M.: Dynamics of Sediments in Reservoir Inflows: A Case Study of the Skalka and Nechranice Reservoirs, Czech Republic, *ISPRS International Journal of Geo-Information*, 9, <https://doi.org/10.3390/ijgi9040258>, 2020.
- 1360 Panagos, P., Borrelli, P., Poesen, J., Ballabio, C., Lugato, E., Meusburger, K., Montanarella, L., and Alewell, C.: The new assessment of soil loss by water erosion in Europe, *Environmental Science & Policy*, 54, 438–447, <https://doi.org/10.1016/j.envsci.2015.08.012>, 2015.
- Papini, M., Ivanov, V., Brambilla, D., Arosio, D., and Longoni, L.: Monitoring bedload sediment transport in a pre-Alpine river: An experimental method, *Rendiconti Online della Società Geologica Italiana*, 43, 57–63, 1365 <https://doi.org/10.3301/ROL.2017.35>, 2017.
- Parenti, C., Rossi, P., Mancini, F., Scorpio, V., Grassi, F., Ciccarese, G., Lugli, F., and Soldati, M.: Multitemporal Analysis of Slow-Moving Landslides and Channel Dynamics through Integrated Remote Sensing and In Situ Techniques, *Remote Sensing*, 15, <https://doi.org/10.3390/rs15143563>, 2023.
- Pearson, E., Smith, M. W., Klaar, M. J., and Brown, L. E.: Can high resolution 3D topographic surveys provide 1370 reliable grain size estimates in gravel bed rivers?, *Geomorphology*, 293, 143–155, <https://doi.org/10.1016/j.geomorph.2017.05.015>, 2017.
- Pebesma, E. J., de Jong, K., and Briggs, D.: Interactive visualization of uncertain spatial and spatio-temporal data under different scenarios: an air quality example, *International Journal of Geographical Information Science*, 21, 515–527, <https://doi.org/10.1080/13658810601064009>, 2007.
- 1375 Peirce, S., Ashmore, P., and Leduc, P.: Evolution of grain size distributions and bed mobility during hydrographs in gravel-bed braided rivers, *Earth Surface Processes and Landforms*, 44, 304–316, <https://doi.org/10.1002/esp.4511>, 2019.
- Pelletier, J. D., Broxton, P. D., Hazenberg, P., Zeng, X., Troch, P. A., Niu, G.-Y., Williams, Z., Brunke, M. A., and Gochis, D.: A gridded global data set of soil, intact regolith, and sedimentary deposit thicknesses for regional and 1380 global land surface modeling, *Journal of Advances in Modeling Earth Systems*, 8, 41–65, <https://doi.org/10.1002/2015MS000526>, 2016.
- Pereira, S., Garcia, R., Zêzere, J., Oliveira, S., and Silva, M.: Landslide quantitative risk analysis of buildings at the municipal scale based on a rainfall triggering scenario, *Geomatics, Natural Hazards and Risk*, 8, <https://doi.org/10.1080/19475705.2016.1250116>, 2016.
- 1385 Pérez-Peña, J. V., Azañón, J. M., and Azor, A.: CalHypso: An ArcGIS extension to calculate hypsometric curves and their statistical moments. Applications to drainage basin analysis in SE Spain, *Computers & Geosciences*, 35, 1214–1223, 2009.
- Rahardjo, H., Satyanaga, A., Leong, E. C., Santoso, V. A., and Ng, Y. S.: Performance of an instrumented slope covered with shrubs and deep-rooted grass, *Soils and Foundations*, 54, 417–425, 1390 <https://doi.org/10.1016/j.sandf.2014.04.010>, 2014.
- Raj, P. P.: Comparison of True and Residual Friction Angles, *Soils and Foundations*, 21, 99–103, [https://doi.org/10.3208/sandf1972.21.3\\_99](https://doi.org/10.3208/sandf1972.21.3_99), 1981.

- Ravi, V., Williams, J. R., and Ouyang, Y.: Estimation of infiltration rate in the vadose zone: compilation of simple mathematical models, 1998.
- 1395 Raziiei, T. and Pereira, L.: Estimation of ETo with Hargreaves-Samani and FAO-PM temperature methods for a wide range of climates in Iran, *Agricultural Water Management*, 121, 1–18, <https://doi.org/10.1016/j.agwat.2012.12.019>, 2013.
- Remondo, J., Bonachea, J., and Cendrero, A.: A statistical approach to landslide risk modelling at basin scale: From landslide susceptibility to quantitative risk assessment, *Landslides*, 2, 321–328, <https://doi.org/10.1007/s10346-005-0016-x>, 2005.
- 1400 Rickenmann, D.: Empirical Relationships for Debris Flows, *Natural Hazards*, 19, 47–77, <https://doi.org/10.1023/A:1008064220727>, 1999.
- Rocha, J., Duarte, A., Silva, M., Fabres, S., Vasques, J., Revilla-Romero, B., and Quintela, A.: The Importance of High Resolution Digital Elevation Models for Improved Hydrological Simulations of a Mediterranean Forested Catchment, *Remote Sensing*, 12, <https://doi.org/10.3390/rs12203287>, 2020.
- 1405 Ronchetti, F., Borgatti, L., Cervi, F., C. G., Piccinini, L., Vincenzi, V., and Alessandro, C.: Groundwater processes in a complex landslide, northern Apennines, Italy, *Natural Hazards and Earth System Sciences*, 9, 895–904, <https://doi.org/10.5194/nhess-9-895-2009>, 2009.
- Roo, A., A.P.J, Wesseling, C. G., Jetten, V. G., and Ritsema, C.: LISEM: A physically-based hydrological and soil erosion model incorporated in a GIS, In: K. Kovar & H.P. Nachtnebel (eds.), *Application of geographic information systems in hydrology and water resources management*. Wallingford (UK), IAHS, 1996. IAHS Publ. 235, pp. 395-403, 1996.
- 1410 Ross, C. W., Prihodko, L., Anchang, J., Kumar, S., Ji, W., and Hanan, N. P.: HYSOGs250m, global gridded hydrologic soil groups for curve-number-based runoff modeling, *Sci Data*, 5, 180091–180091, <https://doi.org/10.1038/sdata.2018.91>, 2018.
- 1415 Salles, T.: eSCAPE: Regional to global scale landscape evolution model v2. 0, 2019.
- Sambrook Smith, G. H. and Ferguson, R. I.: The gravel-sand transition along river channels, *Journal of Sedimentary Research*, 65, 423–430, <https://doi.org/10.1306/D42680E0-2B26-11D7-8648000102C1865D>, 1995.
- Scheidl, C. and Rickenmann, D.: TopFlowDF - A simple gis based model to simulate debris-flow runout on the fan, <https://doi.org/10.4408/IJEGE.2011-03.B-030>, 2011.
- 1420 Schellekens, J., Verseveld, W. van, Visser, M., hcwinsemius, laurenebouaziz, tanjaeuser, sandercdevries, cthiange, hboisgon, DirkEilander, DanielTollenaar, aweerts, Baart, F., Pieter9011, Pronk, M., arthur-lutz, ctenvelden, Imme1992, and Jansen, M.: *openstreams/wflow: Bug fixes and updates for release 2020.1.2*, Zenodo, <https://doi.org/10.5281/zenodo.4291730>, 2020.
- 1425 Schoener, G. and Stone, M. C.: Monitoring soil moisture at the catchment scale – A novel approach combining antecedent precipitation index and radar-derived rainfall data, *Journal of Hydrology*, 589, 125155, <https://doi.org/10.1016/j.jhydrol.2020.125155>, 2020.
- Shobe, C., Tucker, G., and Barnhart, K.: The SPACE 1.0 model: A Landlab component for 2-D calculation of sediment transport, bedrock erosion, and landscape evolution, *Geoscientific Model Development Discussions*, 1–38, <https://doi.org/10.5194/gmd-2017-175>, 2017.
- 1430 Sklar, L. S., Riebe, C. S., Marshall, J. A., Genetti, J., Leclere, S., Lukens, C. L., and Merces, V.: The problem of predicting the size distribution of sediment supplied by hillslopes to rivers, *Geomorphology*, 277, 31–49, 2017.
- Smith, R. E. and Parlange, J.-Y.: A parameter-efficient hydrologic infiltration model, *Water Resources Research*, 14, 533–538, <https://doi.org/10.1029/WR014i003p00533>, 1978.
- 1435 Strahler, A. N.: Dynamic basis of geomorphology, *Geological society of america bulletin*, 63, 923–938, 1952.

- Strauch, R., Istanbuloglu, E., Nudurupati, S. S., Bandaragoda, C., Gasparini, N. M., and Tucker, G. E.: A hydroclimatological approach to predicting regional landslide probability using Landlab, *Earth Surf. Dynam.*, 6, 49–75, <https://doi.org/10.5194/esurf-6-49-2018>, 2018.
- 1440 Sutanudjaja, E. H., van Beek, R., Wanders, N., Wada, Y., Bosmans, J. H. C., Drost, N., van der Ent, R. J., de Graaf, I. E. M., Hoch, J. M., de Jong, K., Karssenber, D., López López, P., Peßenteiner, S., Schmitz, O., Straatsma, M. W., Vannamettee, E., Wisser, D., and Bierkens, M. F. P.: PCR-GLOBWB 2: a 5\,arcmin global hydrological and water resources model, *Geoscientific Model Development*, 11, 2429–2453, <https://doi.org/10.5194/gmd-11-2429-2018>, 2018.
- 1445 Takahashi, T.: A Review of Japanese Debris Flow Research, *International Journal of Erosion Control Engineering*, 2, <https://doi.org/10.13101/ijece.2.1>, 2009.
- Tangi, M., Schmitt, R., Bizzi, S., and Castelletti, A.: The CASCADE toolbox for analyzing river sediment connectivity and management, *Environmental Modelling & Software*, 119, 400–406, <https://doi.org/10.1016/j.envsoft.2019.07.008>, 2019.
- 1450 Tanyaş, H., van Westen, C. J., Allstadt, K. E., and Jibson, R. W.: Factors controlling landslide frequency–area distributions, *Earth Surface Processes and Landforms*, 44, 900–917, <https://doi.org/10.1002/esp.4543>, 2019.
- Tavares da Costa, R., Mazzoli, P., and Bagli, S.: Limitations Posed by Free DEMs in Watershed Studies: The Case of River Tanaro in Italy, *Frontiers in Earth Science*, 7, 141, <https://doi.org/10.3389/feart.2019.00141>, 2019.
- 1455 Terzago, S., Palazzi, E., and von Hardenberg, J.: Stochastic downscaling of precipitation in complex orography: a simple method to reproduce a realistic fine-scale climatology, *Nat. Hazards Earth Syst. Sci.*, 18, 2825–2840, <https://doi.org/10.5194/nhess-18-2825-2018>, 2018.
- Theule, J.: Geomorphic study of sediment dynamics in active debris-flow catchments (French Alps), 2012.
- Tóth, B., Weynants, M., Pásztor, L., and Hengl, T.: 3D soil hydraulic database of Europe at 250 m resolution, *Hydrological Processes*, 31, 2662–2666, <https://doi.org/10.1002/hyp.11203>, 2017.
- 1460 Trambly, Y., Bouvier, C., Martin, C., Didon-Lescot, J.-F., Todorovik, D., and Domergue, J.-M.: Assessment of initial soil moisture conditions for event-based rainfall–runoff modelling, *Journal of Hydrology*, 387, 176–187, <https://doi.org/10.1016/j.jhydrol.2010.04.006>, 2010.
- Uber, M., Vandervaere, J.-P., Zin, I., Braud, I., Heistermann, M., Legoût, C., Molinié, G., and Nord, G.: How does initial soil moisture influence the hydrological response? A case study from southern France, *Hydrology and Earth System Sciences*, 22, 6127–6146, <https://doi.org/10.5194/hess-22-6127-2018>, 2018.
- 1465 Vakhshoori, V. and Zare, M.: Is the ROC curve a reliable tool to compare the validity of landslide susceptibility maps?, *null*, 9, 249–266, <https://doi.org/10.1080/19475705.2018.1424043>, 2018.
- Van Der Knijff, J. M., Younis, J., and De Roo, A. P. J.: LISFLOOD: a GIS-based distributed model for river basin scale water balance and flood simulation, *null*, 24, 189–212, <https://doi.org/10.1080/13658810802549154>, 2010.
- 1470 Van Genuchten, M.: A Closed-form Equation for Predicting the Hydraulic Conductivity of Unsaturated Soils1, *Soil Science Society of America Journal*, 44, <https://doi.org/10.2136/sssaj1980.03615995004400050002x>, 1980.
- de Vente, J. and Poesen, J.: Predicting soil erosion and sediment yield at the basin scale: Scale issues and semi-quantitative models, *Earth-Science Reviews*, 71, 95–125, <https://doi.org/10.1016/j.earscirev.2005.02.002>, 2005.
- 1475 Vetsch, D., Siviglia, A., Caponi, F., Ehrbar, D., Gerke, E., Kammerer, S., Koch, A., Peter, S., Vanzo, D., Vonwiller, L., Facchini, M., Gerber, M., Volz, C., Farshi, D., Mueller, R., Rousselot, P., Veprek, R., and Faeh, R.: System Manuals of BASEMENT Version 2.8, 2018.
- Vitvar, T., Burns, D. A., Lawrence, G. B., McDonnell, J. J., and Wolock, D. M.: Estimation of baseflow residence times in watersheds from the runoff hydrograph recession: method and application in the Neversink watershed, Catskill Mountains, New York, *Hydrological Processes*, 16, 1871–1877, <https://doi.org/10.1002/hyp.5027>, 2002.

- 1480 Yu, B., Xie, C., Cai, S., Chen, Y., Lv, Y., Mo, Z., Liu, T., and Yang, Z.: Effects of Tree Root Density on Soil Total Porosity and Non-Capillary Porosity Using a Ground-Penetrating Tree Radar Unit in Shanghai, China, *Sustainability*, 10, <https://doi.org/10.3390/su10124640>, 2018.
- Zhang, H., Li, Z., Saifullah, M., Li, Q., and Li, X.: Impact of DEM Resolution and Spatial Scale: Analysis of Influence Factors and Parameters on Physically Based Distributed Model, *Advances in Meteorology*, 2016, 8582041, <https://doi.org/10.1155/2016/8582041>, 2016.
- 1485 Zheng, S., Zhang, G., Yuan, X., Ye, F., and Fu, W.: Failure characteristics of shallow soil slope considering surface runoff and interstitial flow, *Geomatics, Natural Hazards and Risk*, 11, 845–868, <https://doi.org/10.1080/19475705.2020.1758222>, 2020.
- 1490 Zomlot, Z., Verbeiren, B., Huysmans, M., and Batelaan, O.: Spatial distribution of groundwater recharge and base flow: Assessment of controlling factors, *Journal of Hydrology: Regional Studies*, 4, 349–368, <https://doi.org/10.1016/j.ejrh.2015.07.005>, 2015.